Universitat Autònoma
de Barcelona

A Thesis for the

Master in Telecommunication Engineering

Wireless Measurement of Concrete Properties During the Drying Process: Link Budget and Antenna Design

by

Javier Colin Pérez

Supervisor: Josep Parrón Granados

Department of Telecommunications and Systems Engineering

Escola d'Enginyeria
Universitat Autònoma de Barcelona (UAB)

July 2020

El sotasignant, Josep Parrón Granados, Professor de l'Escola d'Enginyeria de la Universitat Autònoma de Barcelona (UAB),

CERTIFICA:

Que el projecte presentat en aquesta memòria de Treball Final de Màster ha estat realitzat sota la seva direcció per l'alumne Javier Colin Pérez.

I, perquè consti a tots els efectes, signa el present certificat.

Bellaterra, 9 de juliol de 2020.

Signatura: Josep Parrón Granados

Abstract

The use of concrete as a constructive element has been involved in many structures and buildings from its invention to the present day. Over time, it has become the most widely used structural material for its easy manufacturing, strength and durability at a very affordable cost. However, despite the obvious importance of this material and its widespread use, the manufacturing, placement or curing procedures in some cases are not adequate, directly affecting its behaviour and quality.

The knowledge of its weaknesses allows the creation of safe and durable structures. That is why nowadays, a great deal of interest is being put into the design of devices capable of working embedded in media such as concrete or other building materials, thus allowing the monitorization of the compound status during the drying process. Nevertheless, a problem that must always be dealt with when designing such devices is the change of the electromagnetic properties of the material.

During the drying process, characteristics of the medium such as dielectric constant or conductivity are strongly affected by the water-to-cement ratio (w/c-ratio). Depending on the state of the medium, they might not only exhibit very high values, but also be variable with time, which affects the matching of an antenna placed inside.

Therefore, the integrated antenna must be able to follow the changes produced in the medium, which means exhibiting a good matching in a certain range of values of the electromagnetic constants of the material. There are ultra-wideband (UWB) solutions in order to have a bandwidth large enough to cover the variation in the permittivity of the material, however, it would be much simpler if it was possible to design an antenna capable of working in the extremes of the changing properties of the medium.

This project aims to design an antenna capable of supporting the change of medium, in this case, of concrete, allowing to send information of interest in any state during its drying process. This information can be collected with a sensor inside the concrete and sent to a reader in free space, outside, via a wireless link at the frequency of 868 MHz (UHF RFID). The analysis of the different states of the medium, leads to the detection of flaws, cracks, defects, voids, inhomogeneities, moisture content, etc., thus avoiding a concrete of poor quality and, consequently, weak and vulnerable architectures.

Resumen

El uso del hormigón como elemento constructivo ha estado presente en multitud de estructuras y edificaciones desde su invención hasta nuestros días. A través del tiempo, se ha convertido en el material estructural más utilizado por su fácil fabricación, resistencia y durabilidad a un coste muy asequible. Sin embargo, a pesar de la evidente importancia de este material y de su uso tan extendido, los procedimientos de elaboración, colocación o curado en algunos casos no son los adecuados, afectando de manera directa el comportamiento y calidad de este.

El conocimiento de sus debilidades permite elaborar estructuras seguras y duraderas. Es por ello que hoy en día, se está poniendo mucho interés en el diseño de dispositivos capaces de trabajar incrustados en medios como el hormigón u otros materiales de construcción, permitiendo así, monitorizar el estado del compuesto durante el proceso de secado. Sin embargo, un problema que siempre debe abordarse al diseñar dichos dispositivos es el cambio en las propiedades electromagnéticas del material.

Durante el proceso de secado, características del medio como la constante dieléctrica o la conductividad, se ven fuertemente afectadas por la relación agua/cemento (*w/c-ratio*). Dependiendo del estado del medio, podrían no solo exhibir valores muy altos, sino también variables con el tiempo, lo que afecta la adaptación de una antena colocada en su interior.

Por lo tanto, la antena integrada debe ser capaz de seguir los cambios producidos en el medio, lo que significa exhibir una buena adaptación en un cierto rango de valores de las constantes electromagnéticas del material. Existen soluciones de banda ultra-ancha (*UWB*) con el objetivo de tener un ancho de banda lo suficientemente grande como para cubrir la variación en la permitividad del material, no obstante, sería mucho más simple si fuera posible, diseñar una antena capaz de trabajar en los extremos de las propiedades cambiantes del medio.

Este proyecto persigue el objetivo de diseñar una antena capaz de soportar el cambio de medio, en este caso, del hormigón, permitiendo enviar información de interés en cualquier estado de este durante su proceso de secado. Dicha información puede ser recogida con un sensor en el interior del hormigón y enviada a un lector en espacio libre, al exterior, mediante un enlace inalámbrico a la frecuencia de 868 MHz (UHF RFID). El análisis de los diferentes estados del medio, conduce a la detección de fallas, grietas, defectos, huecos, falta de homogeneidad, contenido de humedad, etc., evitando así, un hormigón de mala calidad y en consecuencia, arquitecturas débiles y vulnerables.

Agradecimientos

Después de finalizar esta tesis, me siento en deuda con muchas personas que de manera directa o indirecta han contribuido en este trabajo. Su ayuda y sus consejos, han sido fundamentales para completar esta etapa del máster que ahora termina.

Mi primer agradecimiento va para mi director de tesis, Josep Parrón Granados, por la confianza, la motivación e implicación que me ha demostrado durante este tiempo. A parte de transmitirme su experiencia y conocimientos en este trabajo, él ha sido el principal responsable de despertar mi interés sobre el mundo de las antenas desde el grado.

A Ernesto Díaz, por su profesionalidad en las tareas de laboratorio. La fabricación de la antena y los consejos sobre la elaboración del cemento han sido clave en este proyecto.

Finalmente, a mi familia empezando por mis hermanos Ricardo y Dani. Gracias Ricardo, por compartir conmigo todas esas tardes de estudios que parecían infinitas durante los seis años de Universidad. Contigo han sido mucho más llevaderas y hemos formado un gran equipo. Gracias Dani, por tu figura de hermano mayor y poder contar con tu ayuda siempre que lo hemos necesitado. Gracias a mis padres, por ayudarme a cumplir mis objetivos como persona y estudiante. Laura, por esa capacidad tuya de estar siempre de buen humor, con una sonrisa, quitando importancia a las cosas y animándome hasta el final.

Javier Colin Pérez
27 de junio de 2020

Contents

List of Figures

List of Tables

Chapter 1

Introduction

1.1 Motivation and Objectives

The durability of concrete constructions can be seriously affected by chemical and physical phenomena and other causes such as design errors, poor execution during construction or ageing effects. Despite the fact that engineering components or structures are intensively designed against fatigue failures, more than 50 % of mechanical failures are due to fatigue crack [1], which may cause economic losses and jeopardize the human safety. This problem, represents a great economic cost in developed countries because of the large infrastructures built there, both roads and buildings.

Due to the development and maturity of internet of things (IoT), wireless passive sensors are highly desirable to monitor these infrastructures. Although the present dissertation is focused on the particular application concerned with concrete health monitoring, the developed analysis can be related in a conceptually easy fashion to other fields such as antenna design for biomedical purposes, where the medium can be the human body tissue [2]. However, something that makes concrete monitoring different from many other applications with embedded devices is that the working media contains water. This factor makes the task of sending information outwards much more complicated as the antenna is subjected to a medium where the permittivity will vary as a function of time and, therefore, the resonance frequency as well. In the present dissertation, a solution for concrete health monitoring by means of antennas is presented. Thanks to the embedded devices like wireless sensors, it is possible to accommodate them on the antennas to obtain relevant information or properties during the drying process. These properties can be very useful for predicting the structures' life and optimizing the repair strategies. These commented points are the key elements in this project and they lead to the following research lines:

- Determine the permittivity of concrete at 868 MHz. Evaluation of data as a function of time, water content, composition, etc.
- Evaluation of changes in the link budget due to complex permittivity variations of concrete.
- Determine the antenna design in order to reduce the dependence of input impedance with the complex permittivity variations.
- Assess through simulations the validity of the proposed solution.
- Experimental work.

1.2 Thesis Outline

This section provides an outline of the present dissertation with a brief summary of the material presented in each chapter. A schematic presentation is also depicted in Figure 1.

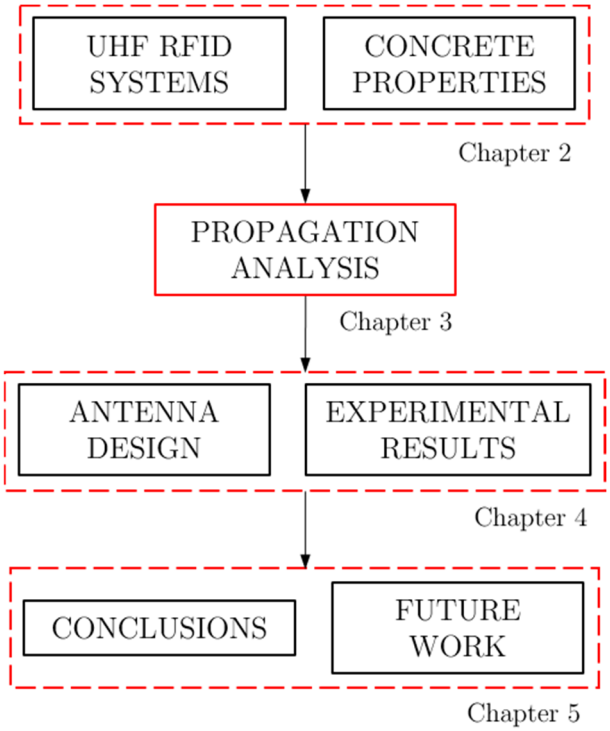

Figure 1: Schematic overview of the topics covered within the present dissertation.

Chapter 2

This chapter is aimed to introduce the reader in the main topics that this thesis will deal with. To this effect, UHF RFID[1] systems are introduced and its possible applications are defined. Besides that, we will justify why the UHF frequency band is better than another for the current application. In addition, information about the state-of-the-art in this type of systems is given to identify the possible contributions of the thesis to the current state of knowledge. On the other side, concrete and its different states are introduced. In this way, the reader is given basic knowledge of concrete and allows us to understand how it works. Defining a series of concrete states is a key task in order to be able to assign a permittivity value to each of these states later on. That is, to recreate the different concrete states, we need the value of permittivity that corresponds to each of them, and that is why it is convenient to define these states from the very beginning.

[1] Radio-frequency identification (RFID) is a form of wireless communication that uses electromagnetic fields to identify and track tags attached to objects. When the tag is triggered by an electromagnetic interrogation pulse from a nearby RFID reader device, the tag transmits digital data back to the reader. Use cases for RFID technology include healthcare, manufacturing, inventory management, etc.

Chapter 3

In this chapter, a propagation analysis is carried out; different scenarios are discussed to understand how the concrete drying process works when an antenna is placed inside it. To do this, multiple simulations are made varying some parameters in order to decide the best or more appropriate value. Based on this, different parameters of interest are selected such as the length of the antenna, the ideal depth, the thickness of the antenna cover, etc. A robust design is important so as not to have too much variation in the results later on. The different conclusions in Chapter 3, give way to the practical work presented in Chapter 4.

Chapter 4

The fourth chapter attempts to design an antenna based on the theory seen earlier. Bringing the design created in FEKO to reality, the simulated model is contrasted with the real antenna to see the variation between them trying to correct certain deviations. In turn, it is useful to corroborate the value of key parameters such as complex permittivity. Chapter 4 also collects the experimental part, i.e., the process that takes to build an antenna and its scenario, where the problems and difficulties that have been mitigated can be seen. For this application, to follow the results, it is recommended to automate measurements so that the working frequency can be monitored as the concrete dries automatically and it is also explained how it has been done. The different tests and adjustments will refine the result to a design good enough to send information from inside the concrete in any state.

1.3 Problem Statement

The use of poor-quality concrete in a construction project can cause loss of structure functionality or even loss of human lives. Furthermore, the concrete is currently one of the most used materials in the construction industry and that is why it is necessary to be continuously updating the knowledge and details of its condition, in order to guarantee a work with quality materials and avoid subsequent unexpected failures – see some examples in Figure 2. Hence, concrete quality has become a very important care factor.

Figure 2: Examples of low-quality concrete.

Since 1970s, developed countries are working to tackling building collapse due to accidents that involve major structural system; these accidents are the abnormal loads not considered in design, extreme environmental effects as well as severe fires [3]. As a real example, the situation in Nigeria can be presented. For over three decades, Nigeria has experienced frequent building failure and collapse; 63 buildings were reported collapsed between 1974 and 2011 with fatality of about 300 [4].

S/N	States	Deaths	Failures	Failure Cause[1]
1	Abuja (FCT)	27	4	PW, Q, SF, PM
2	Benue	1	1	CLSS
3	Cross River	3	1	CLSS
4	Enugu	3	2	NI, Q
5	Imo	2	1	SF
6	Kaduna	41	3	Q, CLSS
7	Kano	Several	1	PM
8	Lagos	132	32	Q, SF, PM, CLSS
9	Nasarawa	2	1	SF
10	Ogun	27	5	Q, PM
11	Ondo	8	1	PS
12	Osun	11	3	Q, SF
13	Oyo	38	7	PM, PW, Q, SF
14	Rivers	-	1	Q

[1] Source [4]. Where, SF–Structural Failure; CLSS–Carelessness; PW–Poor Workmanship; PS–Poor Supervision; PM–Poor Materials; Q–Quackery; NI–Not Investigated.

Table 1: Reported collapsed buildings and deaths according to states in Nigeria 1974-2011 [4].

As it can be seen in Table 1, many of the deaths could have been avoided if the buildings had been built with adequate materials or with a good analysis of the structure before it had been occupied. Moreover, here we only collect results from buildings but concrete is an element that is present in many public places such as roads, which can suppose a great danger if not done carefully. Concerning this, it has also been shown that many motorway accidents are caused by driving on poorly maintained roads. A good concrete manufacturing, brings benefits in terms of road safety, as it reduces the risk of aquaplaning by not accumulating water on the surface and avoiding unexpected potholes or unevenness [5]. Therefore, an increasing demand for reliable inspection and monitoring tools is noticeable. The prediction of the service life of a new structure at the design stage or the diagnosis and the evaluation of the residual service life of existing structures is a key aspect of concrete structure management.

Evaluating the properties of concrete, allows us to know important aspects of its capacity as a construction material. These properties depend on the state in which the material is and

also, depend on the elapsed time. Despite being a changing medium, these valuable properties can be known thanks to a sensor as long as there is an antenna capable of sending the information to the outside for different concrete states. Embedded sensors are meeting the demands for gathering more information from the inside of a structure. Wired sensors are meanwhile well established but may have disadvantages in case of a subsequent installation in existing structures. Wireless sensors which can be embedded in concrete provide an attractive alternative solution.

In this project, we propose the design of a system to send information from inside the concrete to the outside in any state during the drying process by means of an antenna capable of withstanding changes in permittivity. The data of interest can be collected by a sensor, which needs the antenna to send it outside, where the reader is located. Once the information about the status of the concrete has been received, its quality can be analyzed and prevent for any errors on the structures.

1.4 Specifications

This section details the requirements to which the system must fit to make its application possible. These specifications are important not only to define the scope of the system but also to know the characteristics of itself:

- **Operating Frequency**: 868 MHz.
- **Impedance Matching**: Active transmitter with reference impedance of 50 Ω.
- **Size limitations**: Sphere of diameter 5 cm (antenna + board with circuitry and sensors).
- **Radiation Pattern**: As omnidirectional as possible since we will not know in what orientation the sensor will fall into the concrete.

Once defined the specifications that we must meet in our system, we will gradually design it, applying from simple models to confirm link behaviors, to more complex models to be more precise with the final and real result.

Chapter 2

Overview of UHF RFID Systems and Concrete Properties

2.1 Introduction

The purpose of this chapter is to present a general overview of UHF RFID systems and the concrete properties, as well as, the relationship between them that is the key of this project. It is important to define these two great themes separately so we can then see the benefit that brings them together. Due to the wireless and cost-effective characteristics, ultra-high frequency (UHF) radio frequency identification (RFID) tag antenna-based sensors are receiving increasing attention for structural health monitoring. For this, the most advanced UHF RFID systems are introduced, which will make us understand the scope of these and if they are suitable for our application. Afterwards, the concrete properties that are of great interest to the world of construction as well as its different states are shown. Finally, the dielectric properties are analyzed and defined for the different concrete states, something necessary to simulate the work environment. For reference, Figure 3 shows all the ingredients and how they interact with each other.

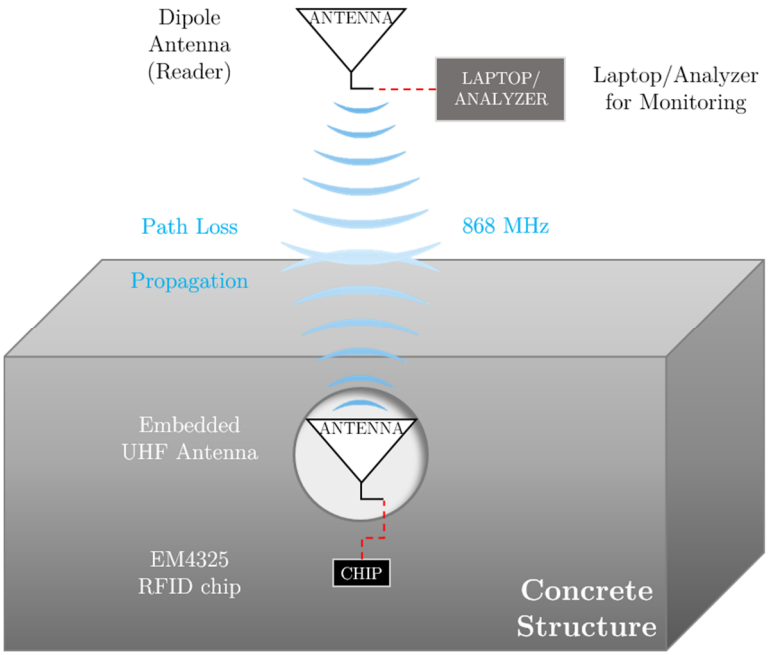

Figure 3: System scheme.

2.2 State-of-the-Art

2.2.1 UHF RFID systems

The fundamental problems of any wireless sensor embedded in concrete are the wireless communication and power consumption. Electromagnetic waves suffer from attenuation in concrete depending on the moisture content, the heterogeneity of concrete, the presence of metal and other factors. Hence, efficient embedded antennas are needed for future wireless structural health monitoring. Since the integration of wireless communication removes the need for transmitting data from one point to another with cables, the lack of cables requires in situ power. Currently, batteries represent the most common portable power source for wireless sensor.

Among the various technologies potentially applicable to our scenario, Radiofrequency Identification (RFID) systems may be a strategic solution thanks to their low-cost and the absence of battery (in some cases – depending on the sensor), which are compatible with disposable application. Moreover, the mode of operation of RFID systems is quite straightforward, in a nutshell; the RFID tag, which contains the identification data of the object to which it is attached, generates a radio frequency signal with said data. This signal can be picked up by an RFID reader, which is responsible for reading the information and passing it in digital format to the specific application that uses RFID. Although RFID's main application is in logistic, it was demonstrated how to extract physical information about the tagged object by transforming the tag antenna itself into a sensor [6], or how to work with RFID antennas on chemical compounds having sensing features [7]. All this leads to have innovatory used systems for different measurement purposes, such as strain detection, material corrosion analysis, crack detection or food quality evaluation [8]. Figure 4 depicts some innovative applications of RFID sensor and the common variables they use for it.

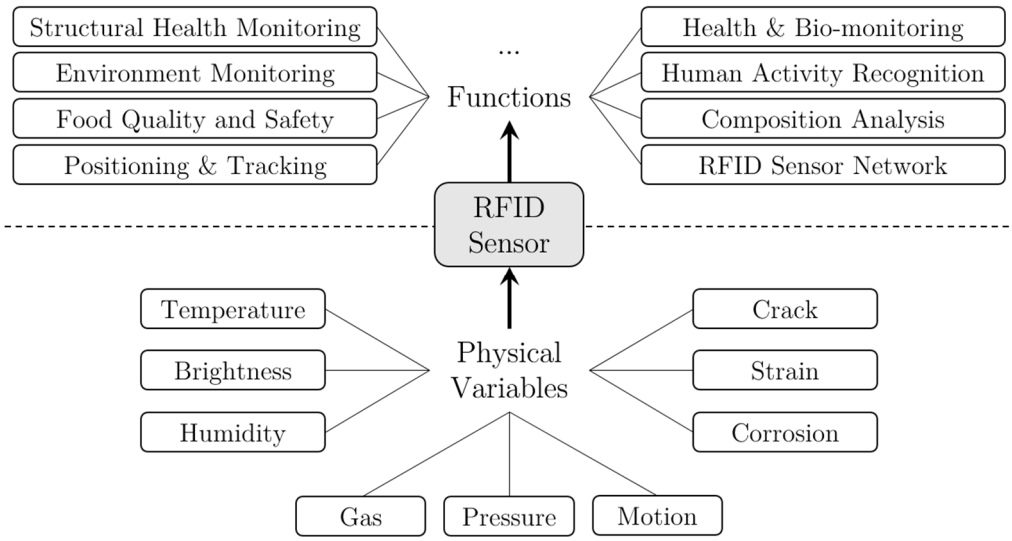

Figure 4: Physical variables and applications of RFID sensors.

A chip widely used in embedded applications is the EM4325 model [9]. It is used in UHF applications operating at 860 MHz – 960 MHz. This chip, is able to work as conventional RFID transponder as well as to provide temperature measurements (an integrated temperature sensor is included, supporting the temperature range from -40 ºC to +60 ºC). The EM4325 is powered either by a battery or by the RF energy transmitted by the reader, which is received and rectified to generate a voltage supply for the device. The temperature readings can be also on demand by a reader or the chip may be programmed to perform self-monitoring with alarm conditions, which makes it very interesting.

The main advantage of UHF transmission band compared with lower transmission bands, is the short wavelength that is due to the high frequency. The size of the transmitting and receiving antennas is related to the size of the wave, in this case microwaves. Therefore, smaller, less cumbersome equipment can be used at high frequency bands. See Figure 5.

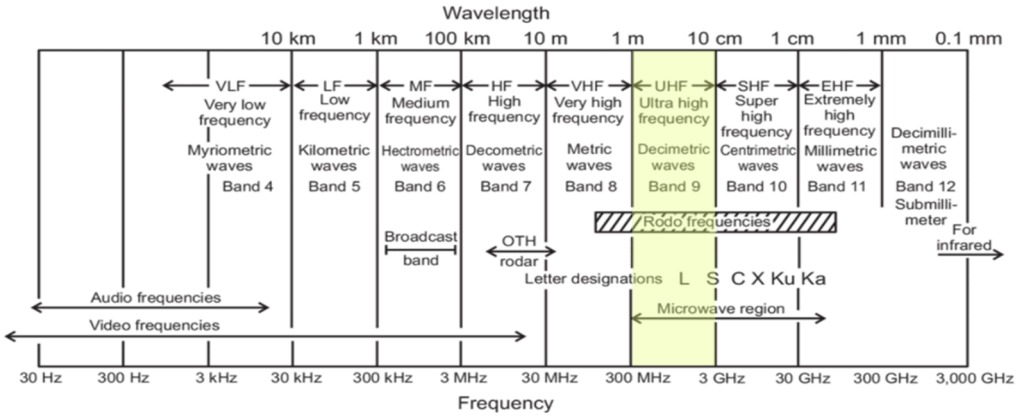

Figure 5: Electromagnetic spectrum [10].

UHF is widely used in transmitting and receiving systems for mobile phones. Transmissions generated by transmitting and receiving radios (transceivers) and mobile phones do not travel far enough to interfere with other local transmissions. This is why UHF radios are commonly used indoors or in areas where a lot of interference can be found, such as buildings and hills. Hence, product identification using the UHF frequency band between 860 and 960 MHz is still key for radio communications because micron-thick antennas are used and because the emission powers of RFID tags do not exceed 200 μW [11], [12]. The emission powers for various electromagnetic wave emitting devices can be compared in Table 2.

Electromagnetic Source	Emission Power
Inlay or RFID Tag	10 – 200 μW
Mobile Phone	Less than 2 W
RFID Antenna	2 W
GSM Base Station	10 – 50 W
FM Radio	300 W
UHF Television	500,000 W

Table 2: Emission power reference for different devices [11].

2.3 Concrete Properties

Concrete is basically a mixture of two components, aggregate and paste. The paste, composed of cement and water, joins the aggregates (sand and gravel or crushed stone) to form a similar mass to a rock when it hardens due to the chemical reaction between the cement and the water. The role of water is important because the water to cement ratio (w/c-ratio) is the most critical factor in the production of "perfect" concrete. Too much water reduces concrete strength, while too little will make the concrete unworkable. Concrete needs to be workable so that it may be consolidated and shaped into different forms (i.e., walls, domes, etc.). Because concrete must be both strong and workable, a careful balance of the cement to water ratio is required when making concrete. The characteristics of the concrete can vary considerably depending on its ingredients. Therefore, for a specific structure, the exact quantities should be used for a good result. The concrete properties are its basic characteristics or qualities. There are four main properties [13]:

- **Workability**: It is an important property for many concrete applications. In essence, it is the ease with which the ingredients can be mixed and the resulting mixture can be handled, transported and placed with little loss of homogeneity.

- **Cohesiveness**: It means how the particles used in the production of concrete are combined together and a good quality of concrete depends on this (quantity of ingredients, quality of materials, etc.). In other words, it is the capability of concrete to remain as a stable and non-segregated dough.

- **Resistance**: It is defined as the capacity to support a load per unit area, and is expressed in terms of effort, usually in kg/cm^2. The universally known test to determine the resistance is the test on cylindrical specimens made in special molds that are 150 mm in diameter and 300 mm high [13].

- **Durability**: The concrete must be able to withstand the weather, the action of chemical products and the damage it will be exposed. The durability of concrete is increased with a good resistance.

These properties are found in different concrete states and depending on how we want to have the concrete, we will be interested to be in one state or another. Here comes into play the sensor, the device in charge of telling us what state it is in. For instance, if we want to make sure that the concrete is in a moldable state because we want to give a specific shape to a structure, we have to work in a state that is neither too fresh nor too hard (i.e. with a certain temperature and humidity). Otherwise, if for example we want to make sure that a floor is ready to build another one on top of it, we will be interested in having it resistant and durable. Therefore, the concrete must be in a hard state, where all the water has

evaporated and consequently with a very low humidity. Thus, parameters such as temperature or humidity provided by the sensor, will help us guess the proper state of the concrete.

From the concrete mass is created until its drying ends, it goes through different states. Figure 6 provides an example of how concrete looks in the distinguished states [13], [14]:

(1) **Fresh state**: At first the concrete looks like a "dough". It is soft and can be worked or molded in different shapes. And so, it is preserved during placement and compaction. The most important properties of fresh concrete are **workability** and **cohesiveness**. (Hydration time[2]: 0 – 6 h)

(2) **Forged/Setting state**: Afterwards, the concrete begins to stiffen. When it is no longer soft, it is known as concrete setting. The setting, takes place after compaction and during finishing. (Hydration time: 6 – 9 h)

(3) **Hardened state**: After concrete has set, it begins to gain resistance and hardens. The properties of hardened concrete are **resistance** and **durability**. (Hydration time: 9 h – until destruction)[3]

Figure 6: Concrete in fresh state, setting state and hardened state respectively.

2.3.1 Dielectric properties of concrete

A dielectric is a material with a low electrical conductivity ($\sigma << 1$ μS/m) that has the capacity to polarize when an electrical field is applied to it [15]. Thus, all dielectric materials are insulators but not all insulators are dielectrics. To design efficient embedded antennas, we need to know the relative permittivity (ε_r) and the conductivity (σ) or the dielectic loss

[2] The water causes the hardening of concrete through a process called hydration. Hydration is a chemical reaction in which the major compounds in cement form chemical bonds with water molecules. In this process, the paste hardens and gains strength to form the rock-like mass known as concrete.
[3] In reference [14], only the first 24 hours of drying are considered – Figure 7. Actually, the hardened state would be until the structure is destroyed.

tanget (tan δ) of concrete, as they, represent the properties of the media through which the waves propagate.

It is well known that the propagation of electromagnetic waves will be affected by the presence of moisture in the concrete. The main obstacle to these electromagnetic waves is the water. Water, an element present in concrete in a high percentage, is one of the elements that blocks the signal. Permittivity is a physical parameter of materials that describes how much they are affected by an electric field. Therefore, the real part of the electrical permittivity and conductivity, will increase with the water content. As we can imagine, our best scenario would be to transmit through the air (without obstacles) where we would have a relative permittivity $\varepsilon r = 1$. So we can anticipate that as the concrete loses water, the permittivity gets closer to that of the air, thus obtaining a better link budget. Figure 7 shows the evolution of dielectric permittivity during 24 hours hydration period at 2.45 GHz [14]. It can be observed that at the initial stage, when the water content in the concrete is high (Hydration time: 0 – 6 h), the dielectic permittivity is high as well. As the hours advance and the drying process progresses, there is less water and therefore a lower dielectric permittivity.

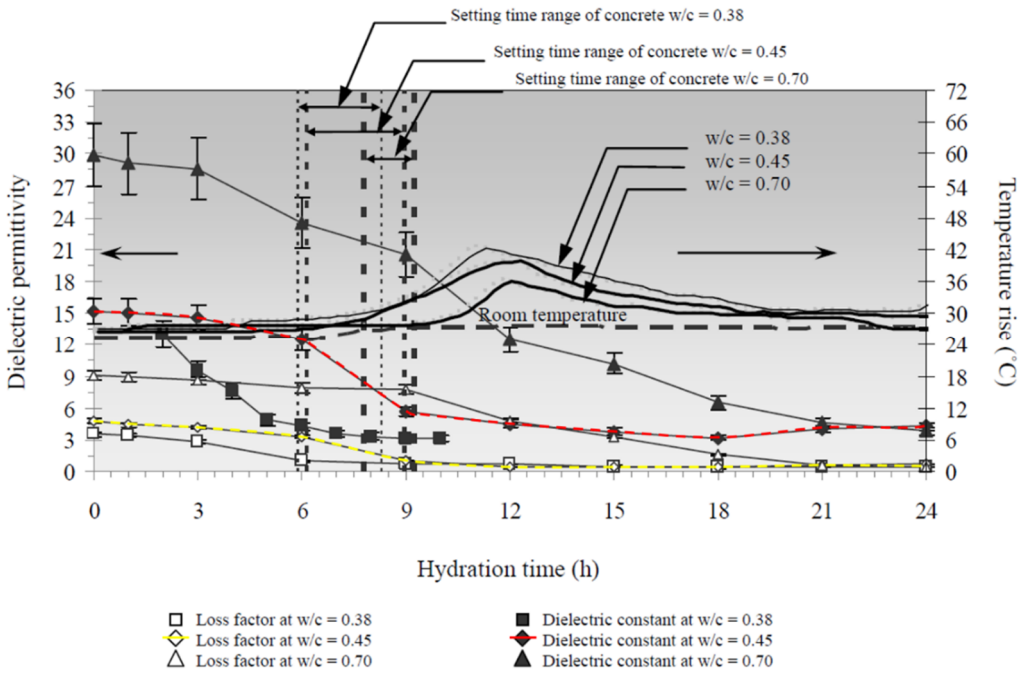

Figure 7: Dielectric permittivity of concrete with different w/c ratios [14].

As the reader can imagine, values such as permittivity or loss tangent of the concrete, can be very variable since it is impossible to obtain equal scenarios (same ingredients, same temperatures, same tracking hours, etc.). Therefore, nowadays there are few sources of information where in turn, the values of these parameters are very diverse and therefore it is difficult to decide which value to use for the design of the antenna. For this, the experimental work is essential, where these values are really tested. For instance, in Figure

7 we can see as a factor such as the water content (w/c), can make the value of the dielectric permittivity significantly different – when concrete is ready for the drying (Hydration time: 0h) for a w/c = 0.45 we will have a dielectric constant of 15 while when the w/c = 0.70, we will have a value of 30. That is why it is risky to rely on a source of information. Not only for its variety in the results but also for the difficulty that supposes to monitor a medium that its properties change sensibly according to the used materials and in turn, as the hours go through.

However, among the limited information available, Natt Makul from Phranakhon Rajabhat University (Bangkok, Thailand), carries out an elaborated study of the behavior of concrete and other cement-based elements in [14]. In addition, he relies on a book that contains information from authentic and highly regarded sources [16]. Despite Figure 7 shows dielectric values of concrete at 2.45 GHz whilst we are interested in 868 MHz, it does not matter since as we can observe in Figure 8 from [16], the variation both the dielectric constant and loss factor of the concrete is very slightly with an increase in microwave frequency. Therefore, [14] is still a good reference.

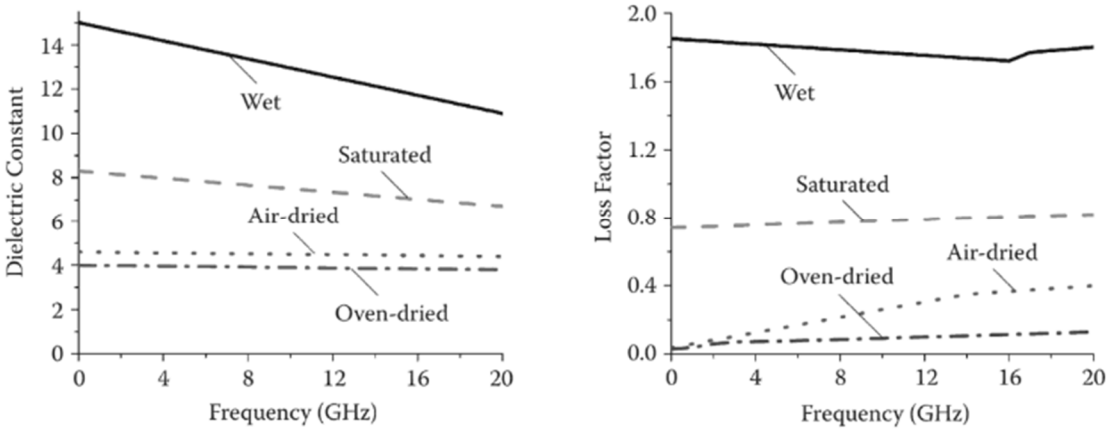

Figure 8: Dielectric constant and loss factor of a typical concrete at microwave frequency range [16].

The analysis of [14] shows the evolution of permittivity in concrete for different w/c. In our experiment we consider w/c = 0.45 not only because it is the mean value but also because the chart values coincide with those of [16] for a regular concrete (Figure 8). To facilitate the visualization, the curve of the dielectric constant ($\varepsilon r'$) and loss factor ($\varepsilon r''$) for w/c = 0.45 has been highlighted in red and yellow respectively in Figure 7.

The relative permittivity (εr) is a complex number given by $\varepsilon r = \varepsilon r' - j\varepsilon r''$. The dielectric loss factor ($\varepsilon r''$) is related to the complex relative permittivity and is a measure of the loss of energy in a dielectric material through conduction, slow polarization currents and other dissipative phenomena. Loss tangent, is defined as $\tan \delta = \varepsilon r''/\varepsilon r'$, and represents how lossy the material is.

Hence, two important equations to consider [17]:

$$\varepsilon r = \varepsilon r' - j\varepsilon r'' \quad (1)$$

$$\tan \delta = \varepsilon r''/\varepsilon r' \quad (2)$$

Based on equations (1) and (2), together with Figure 7, Table 3 has been created. It has been filled in with different parameters of interest every 3 hours during the concrete drying process. These values are the ones we will use later on for the antenna design and the propagation analysis. It is also important to highlight that the antenna is simulated for all 3 states and therefore, a value of permittivity or loss tangent must be chosen to represent each of those states. To do this, the average of each state is made, obtaining a "representative" value for each of the states. This is:

- Fresh State (h = 0 – 6 h): $\varepsilon r' = 14$, $\tan \delta = 0.28$.
- Setting State (h = 6 – 9 h): $\varepsilon r' = 9$, $\tan \delta = 0.25$.
- Hardened State (h = 9 – 24 h): $\varepsilon r' = 4$, $\tan \delta = 0.24$.

The whole data is presented in Table 3.

Concrete state	**Hydration time (h)**	**Dielectric constant ($\varepsilon r'$) w/c = 0.45**	**Loss factor ($\varepsilon r''$) w/c = 0.45**	$\varepsilon r = \varepsilon r' - j\varepsilon r''$	**Loss tangent (tan δ) w/c = 0.45**
Fresh state	0	15	5	15-j5	0.33
	3	14	4	14-j4	0.28
Setting state	6	13	3	13-j3	0.23
	9	7	2	7-j2	0.28
Hardened state	12	6	1	6-j1	0.16
	15	4	1	4-j1	0.25
	18	3	1	3-j1	0.33
	21	5	1	5-j1	0.2
	24	5	1	5-j1	0.2

Table 3: Dielectric properties of concrete during the first 24 hours hydration.

Chapter 3

Simulation Models: Propagation Analysis

3.1 Introduction

Once the key concepts for this project have been seen, we can go through the propagation analysis of the antenna that will be embedded in the concrete. For this purpose, the idea of the full system is introduced at the beginning in a general level in Section 3.2, so that the reader can have a global vision and identify the relevant variables. Later on, we will go deeper into the discussion of how concrete affects the antenna and the link budget. In order to evaluate the system, some figure of merit is needed to tell us how good the link is in the different tests and designs. Therefore, in Section 3.3 we present antenna pair gain, a factor that will be our first reference between models. Finally, we will see the different simulated models that will help to decide the design of the antenna.

3.2 System Description

The system under study is based on two antennas, one embedded inside de concrete, and the other in free space. For guidance, two simple straight dipoles were used (Figure 9).

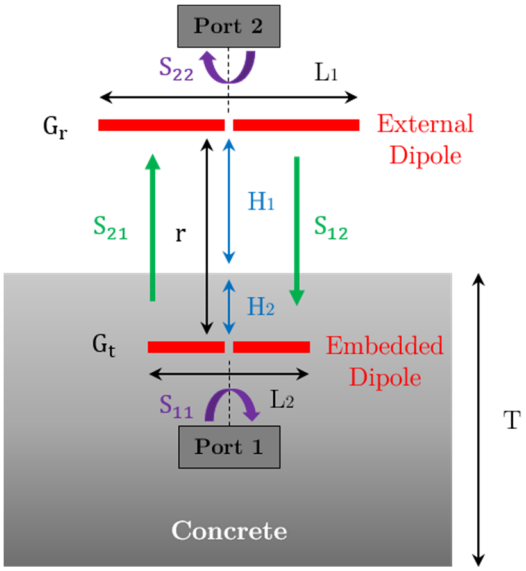

Figure 9: Two half-wavelength resonant dipoles scenario.

They are not the optimal solution, but at least, they can be used as reference. Half-wavelength resonant dipoles are used as transmitter and receiver antennas for better matching. Hence, we can already notice that the electrical length of the embedded antenna will be different depending on the permittivity as wavelength depends also on it:

Free Space $$\lambda_0 = \frac{c_0}{f} \quad (3)$$

Dielectric $$\lambda = \frac{c_0}{f\sqrt{\varepsilon'_r}} \quad (4)$$

Then, embedding the dipole in a dielectric will reduce the size (since the wavelength reduces as well). I.e., the higher the dielectric constant ($\varepsilon r'$), the shorter the wavelength (λ) and thus the smaller the antenna (L_2). Therefore, the antennas' length will be:

External Dipole $$L_1 = \frac{\lambda_0}{2} = \frac{c_0}{2 \cdot f} \approx 17.27 \text{ cm} \quad (5)$$

Embedded Dipole $$L_2 = \frac{\lambda}{2} = \frac{c_0}{2 \cdot f \cdot \sqrt{\varepsilon'_{r\,concrete}}} \approx [4.46 \text{ cm} - 8.63 \text{ cm}] \quad (6)$$

Where f, is the operating frequency, this is 868 MHz and $\varepsilon'_{r\,concrete}$ is the dielectric constant in the concrete. Thus, we can see how the external dipole has a size of about 17.27 cm always (no influence of any medium), while the embedded dipole can vary from 4.46 cm to 8.63 cm because the permittivity varies from 15 to 4 according to Figure 7.

As it has been seen in Section 2.3.1, during the drying process, the water content into the concrete varies; as the concrete dries, it loses water and therefore the permittivity decreases. So, we can realize that there is a trade-off: a high dielectric constant has the advantage of reducing the size of the antenna (compact antenna can be designed), but there will be less radiation[4], hence, gain will decrease.

Then, we can notice that there are many variables to consider (dipole length, distance between dipoles, cover thickness, etc.), which may affect the transmission of data in our system. To understand how these variables behave, different test cases have been prepared. Thanks to these simulations, we try to fix some of the variables in Figure 9 so we can make comparisons and understand better the behaviour of the link-budget.

[4] Any antenna with $L << \lambda$ (small dipoles), regardless its current distribution, has the same directivity pattern ($D_{max} = 1.5$)

3.3 Antenna Pair Gain

Antenna pair gain is the reference we are going to use to evaluate how good the link is. Next, we develop some expressions to show where it comes from. It can be calculated using the scattering parameters of a system. Consider an arbitrary two-port network [S] connected to source and load impedances $\mathrm{Z_s}$ and $\mathrm{Z_L}$, respectively as shown in Figure 10.

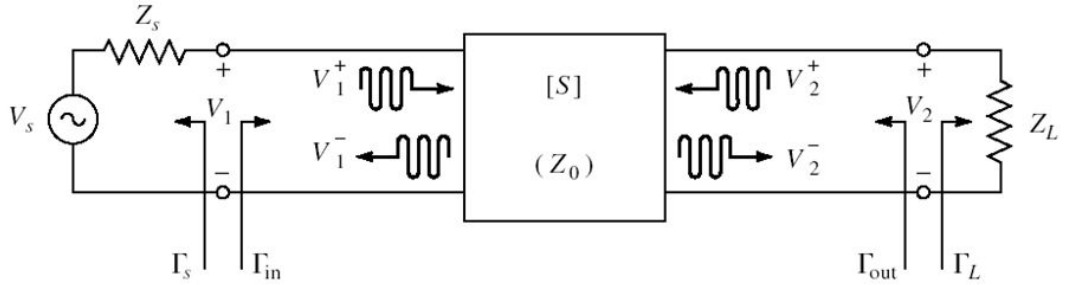

Figure 10: A two-port network with general source and load impedances [18].

The reflection coefficient seen looking toward the load is

$$\Gamma_{\mathrm{L}} = \frac{\mathrm{Z_L} - \mathrm{Z_0}}{\mathrm{Z_L} + \mathrm{Z_0}}, \tag{7a}$$

while the reflection coefficient seen looking toward the source is

$$\Gamma_{\mathrm{S}} = \frac{\mathrm{Z_S} - \mathrm{Z_0}}{\mathrm{Z_S} + \mathrm{Z_0}}, \tag{7b}$$

where $\mathrm{Z_0}$ is the characteristic impedance reference for the S parameters of the two-port network.

From the definition of the S parameters that $\mathrm{V_2^+ = \Gamma_L V_2^-}$, we have

$$\mathrm{V_1^- = S_{11}V_1^+ + S_{12}V_2^+ = S_{11}V_1^+ + S_{12}\Gamma_L V_2^-}\,, \tag{8a}$$

$$\mathrm{V_2^- = S_{21}V_1^+ + S_{22}V_2^+ = S_{21}V_1^+ + S_{22}\Gamma_L V_2^-}\,. \tag{8b}$$

Eliminating $\mathrm{V_2^-}$ from (8a) and solving for $\mathrm{V_1^-/V_1^+}$ gives

$$\Gamma_{\mathrm{in}} = \frac{\mathrm{V_1^-}}{\mathrm{V_1^+}} = \mathrm{S_{11}} + \frac{\mathrm{S_{12}S_{21}\Gamma_L}}{1 - \mathrm{S_{22}\Gamma_L}} = \frac{\mathrm{Z_{in}} - \mathrm{Z_0}}{\mathrm{Z_{in}} + \mathrm{Z_0}}, \tag{9a}$$

where Z_{in} is the impedance seen looking into port 1 of the terminated network. Similarly, the reflection coefficient seen looking into port 2 of the network when port 1 is terminated by Z_S is

$$\Gamma_{out} = \frac{V_2^-}{V_2^+} = S_{22} + \frac{S_{12}S_{21}\Gamma_S}{1 - S_{11}\Gamma_S}. \tag{9b}$$

By voltage division,

$$V_1 = V_S \frac{Z_{in}}{Z_S + Z_{in}} = V_1^+ + V_1^- = V_1^+(1 + \Gamma_{in}).$$

Using

$$Z_{in} = Z_0 \frac{1 + \Gamma_{in}}{1 - \Gamma_{in}},$$

from (9a) and solving for V_1^+ in terms of V_S gives

$$V_1^+ = \frac{V_S}{2} \frac{(1 - \Gamma_S)}{(1 - \Gamma_S\Gamma_{in})}. \tag{10}$$

If peak values are assumed for all voltages, the average power delivered to the network is

$$P_{in} = \frac{1}{2Z_0}|V_1^+|^2(1 - |\Gamma_{in}|^2) = \frac{|V_S|^2}{8Z_0} \frac{|1 - \Gamma_S|^2}{|1 - \Gamma_S\Gamma_{in}|^2}(1 - |\Gamma_{in}|^2), \tag{11}$$

where (10) was used. The power delivered to the load is

$$P_L = \frac{|V_2^-|^2}{2Z_0}(1 - |\Gamma_L|^2). \tag{12}$$

Solving for V_2^- from (8b), substituting into (12), and using (10) gives

$$P_L = \frac{|V_1^+|^2}{2Z_0} \frac{|S_{21}|^2(1 - |\Gamma_L|^2)}{|1 - S_{22}\Gamma_L|^2} = \frac{|V_S|^2}{8Z_0} \frac{|S_{21}|^2(1 - |\Gamma_L|^2)|1 - \Gamma_S|^2}{|1 - S_{22}\Gamma_L|^2|1 - \Gamma_S\Gamma_{in}|^2}. \tag{13}$$

The power available from the source, P_{avs}, is the maximum power that can be delivered to the network. This occurs when the input impedance of the terminated network is conjugately matched to the source impedance. Thus, from (11),

$$P_{avs} = P_{in}\big|_{\Gamma_{in} = \Gamma_S^*} = \frac{|V_S|^2}{8Z_0} \frac{|1 - \Gamma_S|^2}{(1 - |\Gamma_S|^2)}. \tag{14}$$

Finally, from (13) and (14), the transducer power gain is

$$G_T = \frac{P_L}{P_{avs}} = \frac{|S_{21}|^2(1-|\Gamma_S|^2)(1-|\Gamma_L|^2)}{|1-\Gamma_S\Gamma_{in}|^2|1-S_{22}\Gamma_L|^2}. \tag{15}$$

And (15), can be related with the Friis equation [18] were we establish the relationship between the power delivered to the load (P_L), with respect to the one available (P_{avs}), it is what Pozar calls transducer power gain (G_T) in equation (15) at [18]

$$G_T = \frac{P_L}{P_{avs}} = (1-|\Gamma_{in}|^2)G_t\left(\frac{\lambda}{4\pi r}\right)^2 G_r(1-|\Gamma_{out}|^2)\,, \tag{16}$$

where here, G_t is the gain of the transmitting antenna, G_r is the gain of the receiving antenna, λ is the free space wavelength and r is the distance between both antennas.

If the source and load impedances are equal to the reference impedance used to obtain the S-parameters ($Z_s = Z_L = Z_0$), then $\Gamma_s = \Gamma_L = 0$ (equations 7a and b) and additionally, $\Gamma_{in} = S_{11}$ (equation 9a) and $\Gamma_{out} = S_{22}$ (equation 9b), then

$$G_T = \frac{P_L}{P_{avs}} = (1-|S_{11}|^2)G_t\left(\frac{\lambda}{4\pi r}\right)^2 G_r(1-|S_{22}|^2)\,. \tag{17}$$

On the other side, with $Z_s = Z_L = Z_0$, (15) reduces to

$$G_T = \frac{P_L}{P_{avs}} = |S_{21}|^2\,. \tag{18}$$

Matching (17) and (18)

$$\frac{|S_{21}|^2}{(1-|S_{11}|^2)(1-|S_{22}|^2)} = G_t\left(\frac{\lambda}{4\pi r}\right)^2 G_r = G_a\,. \tag{19}$$

And (19) is what is called antenna pair gain [2]. Notice that it models the set of gains and propagation losses that in this scenario are difficult to separate because we are not necessarily in the far field region. The antenna pair gain is one of the main parameters that defines the performance of a wireless system. The terms in the denominator of (19), are used to subtract the mismatch losses of the transmitting and receiving antennas. Therefore, calculating the S-parameters (see Figure 9) for each of the next tests, will tell us the antenna pair gain (19) and thus we will be able to evaluate the link losses for each of the simulations. As expected, we are interested in having G_a as large as possible.

3.4 Multilayer Model: Dipole Depth and Length

In this section a simple multilayer model [19] is used as a first prototype due to its low complexity and low computational cost. In other words, it is a fast way to study the effects of having one antenna embedded in a medium that changes over time. The simulated scenario is shown in Figure 11.

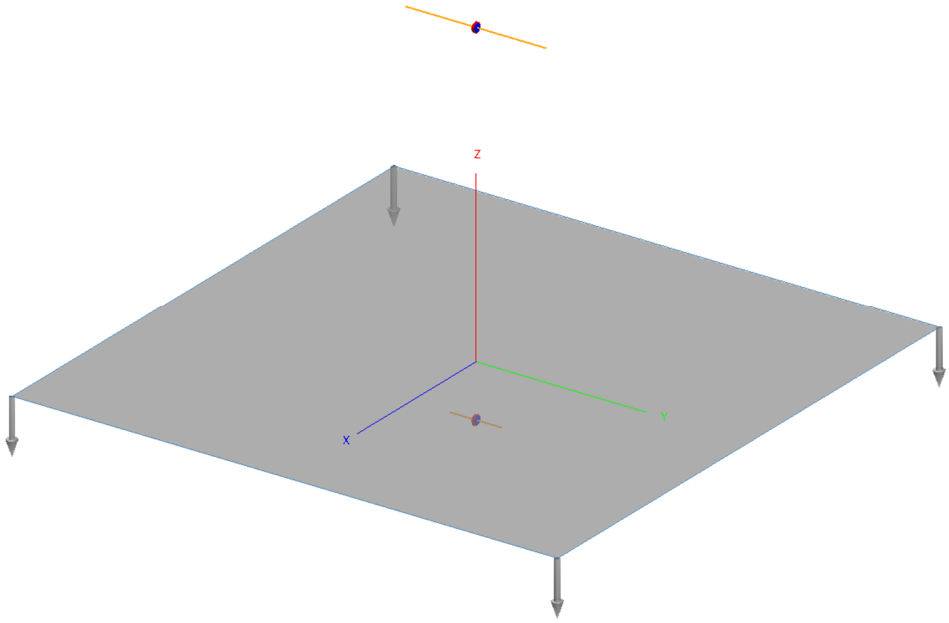

Figure 11: Multilayer model.

It consists in a very straight-forward case where we define two infinite layers/mediums: one layer of free space and the other layer of concrete. This simply structure will provide enough information to decide and define which is the best distance (from the antenna pair gain point of view) to which we must introduce the dipole (H_2) and what is the length of the dipole (L_2) that we must use to work properly in the different drying states of the concrete.

3.4.1 Simulation results

To start-up, a sweep has been made with different values of H_2, the depth at which the dipole is embedded in the concrete. This sweep has been made for the three different states of the concrete, see Table 3 for reference. As it was already introduced in Section 3.2, the dielectric constant will vary the length of the dipole, however, that is something that does not worry us because the antenna pair gain takes into account the mismatch; therefore, the result is the same whatever the length of the dipoles. Then, right now we are just interested in knowing how affects the losses of the link when the distance at which the dipole is embedded changes, regardless of the length of the dipoles.

The result obtained from varying the depth of the dipole inside the concrete from 2 cm to 20 cm is shown in Figure 12 (for details, see Annex A).

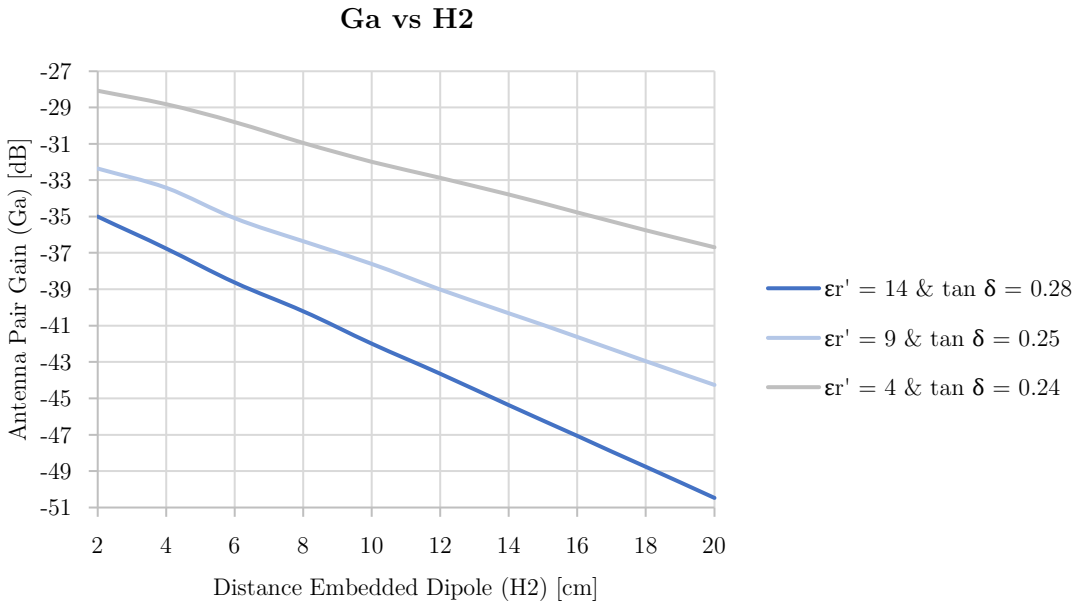

Figure 12: Antenna pair gain as a function of the distance at which the dipole is embedded.

As the dipole is more embedded in the medium, there is a greater distance between antennas, therefore, greater losses and hence, a lower antenna pair gain (G_a). The main difference between the different states is noticed when we double the distance (e.g., from 10 cm to 20 cm), for the fresh state we have more losses (9 dB) than for the other two states (setting and hardened state) where the loss is about 6 dB.

Even though in a real-life scenario the depth at which our antenna falls into the concrete will be difficult to control, we have to determine a value for the coming tests. Considering the specifications defined in Section 1.4, if the antenna's cover must have a diameter of 5 cm, dipping the antenna less than that, would protrude part of the antenna out of the medium. So, we are interested in having the antenna as shallow as possible but as long as it is completely embedded in the concrete. Then, an H_2 = 6 cm is set for the rest of the simulations.

Once we know how depth affects into the losses and fixed the distance for the dipole in the concrete, it is time to define the length of the embedded dipole (L_2). Then, this time a sweep of L_2 is made for the different states, in order to know the value of L_2 that can be used to establish a reliable link for the three concrete states. For this study, although a depth of H_2 = 2 cm will not be simulated, a depth of H_2 = 2 cm and H_2 = 6 cm has been evaluated to have a comparison in different depths of the concrete when the length of the dipole changes. The result is shown in Figure 13 (for details, see Annex A).

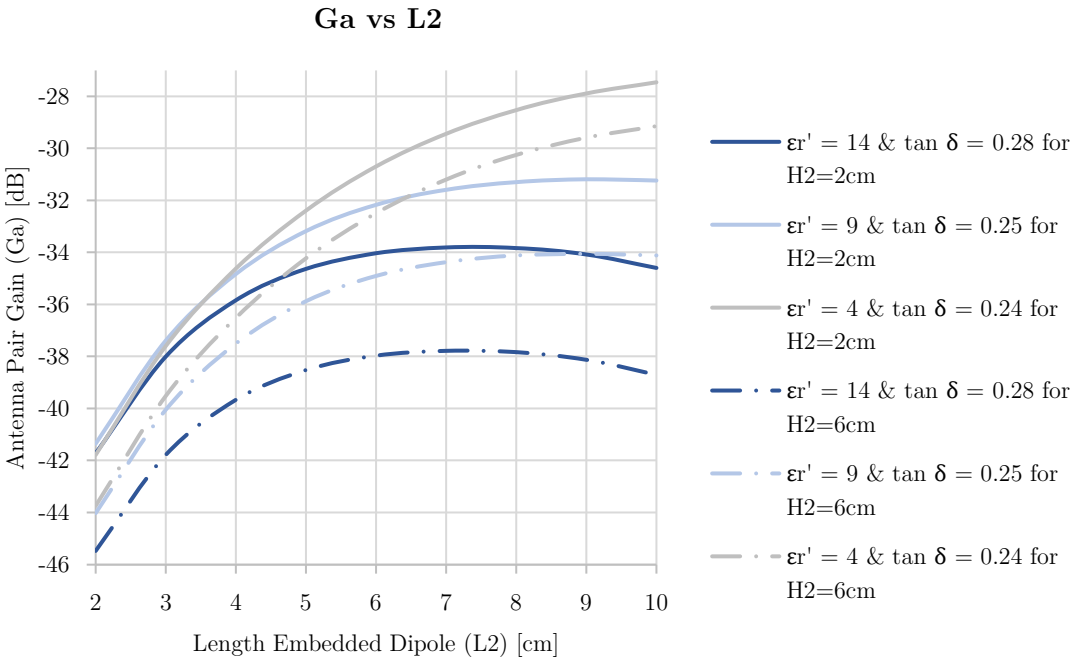

Figure 13: Antenna pair gain as a function of the length of the embedded dipole.

It is easy to see here that for both cases (H_2 = 2 cm and 6 cm) the three states follow the same trend, starting with the worst value of G_a when 2 cm of dipole length is considered (small antennas are poor radiators) and increasing the gain as the antenna size grows. However, there comes a point where having a very large antenna is not going to help us since when the antenna is very long, the maximum radiation will no longer be in the direction of the other dipole and therefore, the G_a starts to decline again.

Therefore, we must rely on taking a value of L_2 that does not exhibit many losses between the three different states (as stable and robust as possible) and at the same time, with a good gain in any state. Looking at the results of Figure 13, a good value, would be 6 cm since it meets with the stated above and also is not too far from the 5 cm that the specifications ask for (in case of needed, miniaturizing the antenna by reducing it 1 cm would not be so difficult).

If we focus in our case, when H_2 = 6 cm, for an L_2 = 6 cm, between any of the 3 states there is only a variation of 5 dB – see Figure 14. In addition, the losses that we have with respect to the best that could be obtained for each one of the states, are not excessive, in particular, for the fresh state where the loss tangent is the highest.

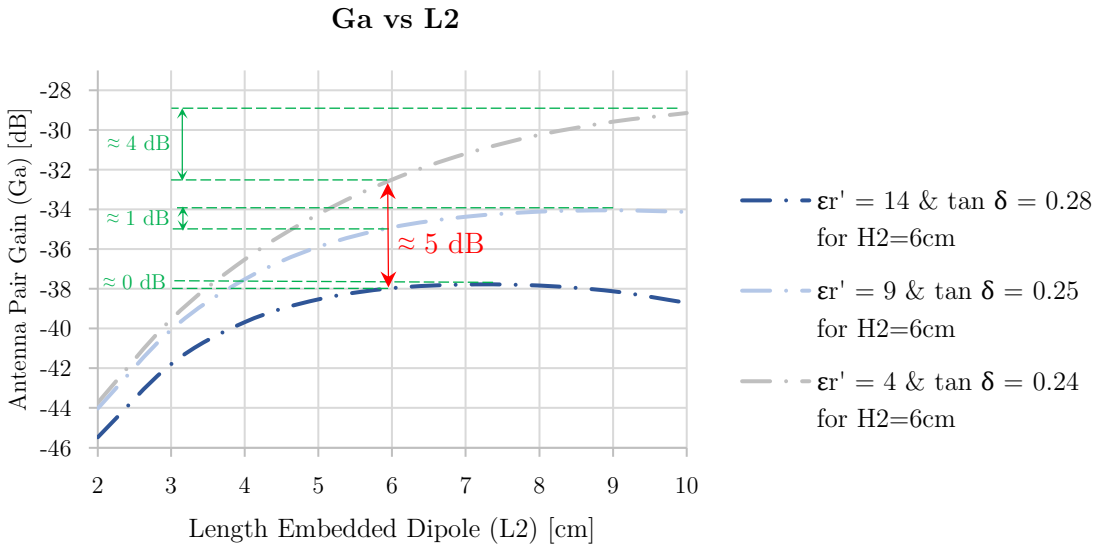

Figure 14: Antenna pair gain as a function of the length of the embedded dipole (analysis for H2 = 6 cm, L2 = 6 cm).

Finally, with the dipole's depth inside the concrete and its length fixed (H_2 = 6 cm and L_2 = 6 cm respectively), we can already analyze how the system behaves over time, that is, as the permittivity decreases (Figure 15).

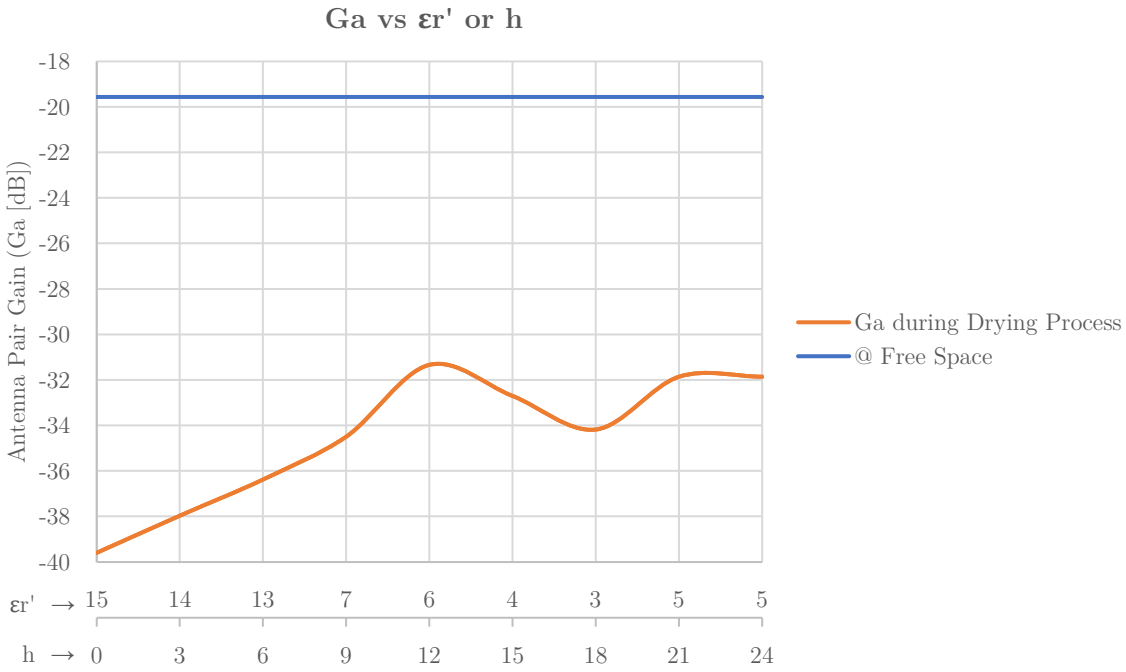

Figure 15: Antenna pair gain during drying process for a multilayer model.

As we can see in Figure 15, as the hours goes by and the concrete loses water, it reduces its permittivity to 5 (the tangent loss also reduces), getting a value much closer to 1, the dielectric constant in free space (or air). The fact that the characteristics of both media are

more similar, causes that the change of medium is not so abrupt and that is why after 24 hours, the losses in the link are minor. Anyway, we also see that it is a quite stable system since from the fresh to the hardened state, the losses have decreased by 8 dB (from -40 dB to -32 dB). Note also that the fact of working with an antenna embedded in a medium, makes us have between 10 dB and 20 dB less compared to free space (for details, see Annex A).

3.5 Multilayer Model with Coating Dipole: Cover Thickness

Now, let us try to improve our model. In order to increase the antenna pair gain, a coating is added to the embedded dipole. The purpose of this coating is to insulate the dipole from the concrete and therefore to smooth the change between the different mediums. It is made with a low-loss dielectric, so now, in the area closest to the antenna (stronger fields) we will not have so many losses and consequently a greater $\mathtt{G_a}$. In this new simulation bank, we use a coated dipole as shown in blue in Figure 16.

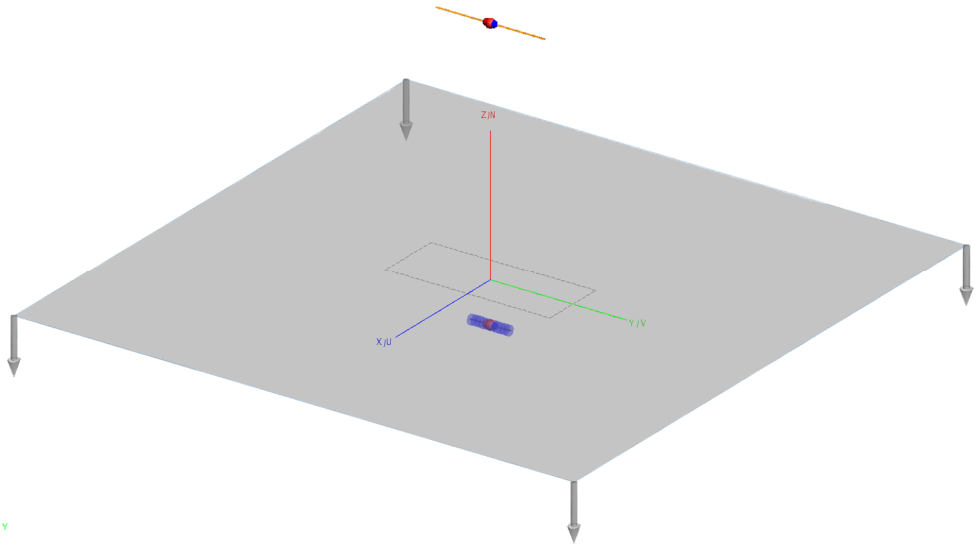

Figure 16: Multilayer model with coating dipole.

The coating chosen is plastic; a manipulable, hard, light-weight and low-cost material. The properties used in the definition of the medium can be found in Table 4.

Substance	Dielectric Constant	Dielectric Strength (V/mil)	Loss Tangent	Max Temp (^{o}F)
ABS (plastic), Molded	3	400 – 1350	0.01	171 – 228

Table 4: Dielectric properties of plastic [20].

3.5.1 Simulation results

As we can see in Figure 17, a sweep has been made increasing the thickness of the plastic cover from 1 mm to 10 mm (this means that for a thickness of 1 mm, the diameter of the coated dipole will be 2 mm, and so on). Especially, it has been beneficial for the section in which there was a valley where the G_a decreased (between 12 and 24 hours of drying). The fact that the dielectric constant of the plastic is equal to the dielectric constant of the concrete for that interval ($\varepsilon r' \approx 3$), has helped to make the transition between mediums much smoother and therefore to have less losses in the link-budget.

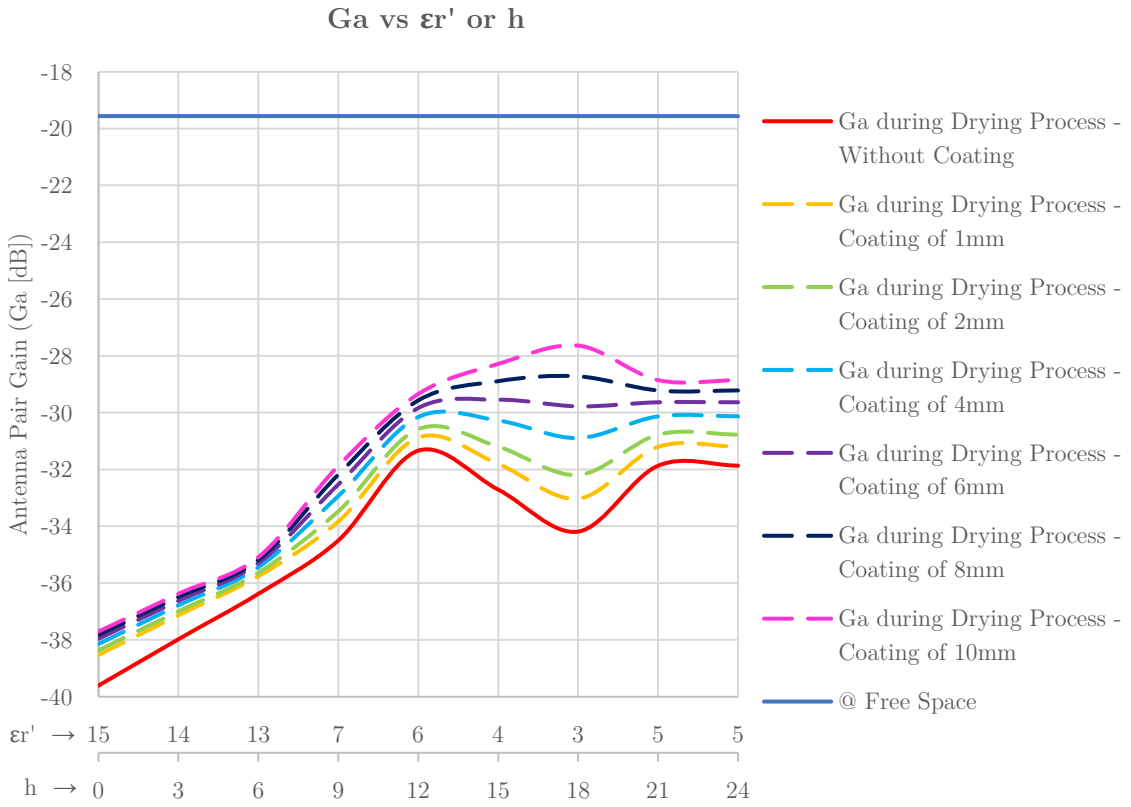

Figure 17: Antenna pair gain as a function of the cover thickness.

Seeing the benefit of a coating with a permittivity similar to that of the medium (see example above when the dielectric constant of the concrete is 3), we thought if this could be applied in other regions, for instance, in the one with a lower antenna pair gain. What would happen if a coating with dielectric constant 12 was used? Would it help to raise this area and make a more uniform slope? Figure 18 shows the result for the fresh state.

As in Figure 17, improvement is achieved for that particular area, but in this case the improvement is only 1 dB and therefore it is not worth (we would be earning 1 dB in fresh state, but losing the improvement in hardened state). For details, see Annex A.

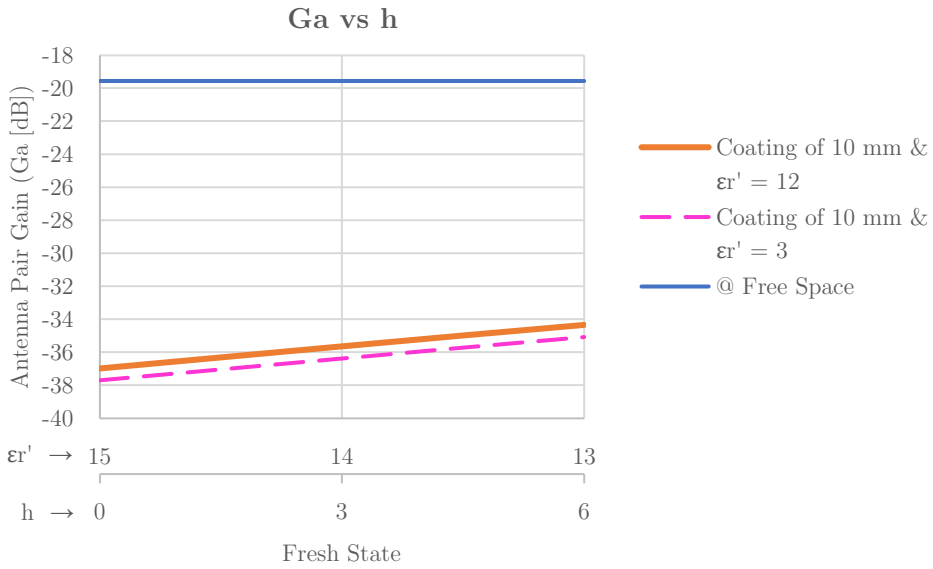

Figure 18: Test for fresh state period – plastic coating with dielectric constant of 12 instead of 3.

Returning to Figure 17, we can also note that the improvement when the thickness of the coating increases, is not very large, so it is not worth using a very thick coating since we are going to have a thicker antenna for a small profit. Then, at most, we could choose a thickness of about 4 or 6 mm, otherwise the design would be worse in terms of size. For the experiment, a cover with a thickness of 1.5 mm will be used because there are not so many losses with respect to using a 4 or 6 mm cover and because it is also the approximate thickness of the FR4 plates. On the other hand, taking into account that the antenna has to be completely covered (both sides), using 1.5 mm plates means a width of 3 mm which is not an exaggerated size.

Thanks to the coating, we have managed to be a little closer to the losses in free space which indicates that we have improved the model. We managed to reduce the losses for all the concrete states, however, we are simulating a non-real model (with infinite concrete). Therefore, it is time to make the model more realistic, so that we can get closer to what we are going to get in a real scenario.

3.6 Multilayer Model with Finite Concrete: Block Thickness

In Figure 19, a concrete thickness of $\mathbf{T} = 20$ cm (see Figure 9 for reference) is defined to be compared against the model with infinite concrete. This change in the model can make the result better or worse as having a finite block with a determined distance, it can introduce signal reflection.

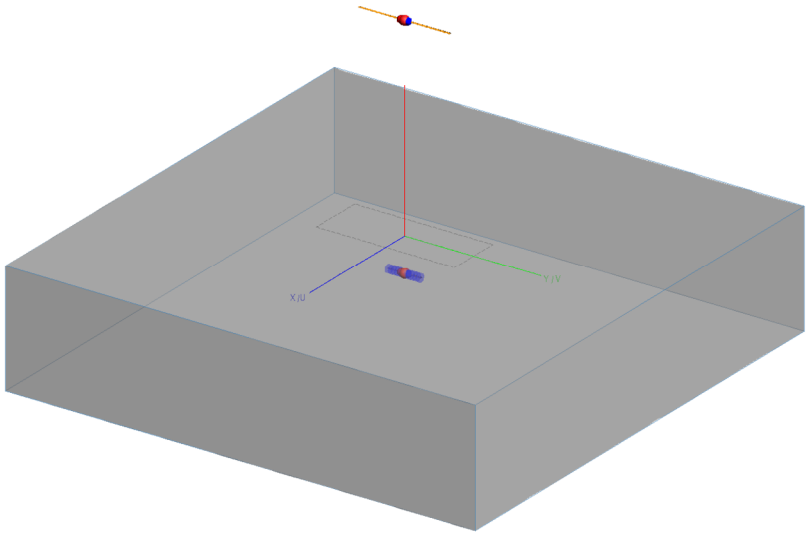

Figure 19: Air-Concrete-Air model with coating dipole.

3.6.1 Simulation results

As we can see in Figure 20, the effect that causes having a finite block instead of an infinite one, is very small thing, that is good. The point at which one model differs more from another has a difference of only 2 dB and, therefore, nothing worrisome. For details, see Annex A.

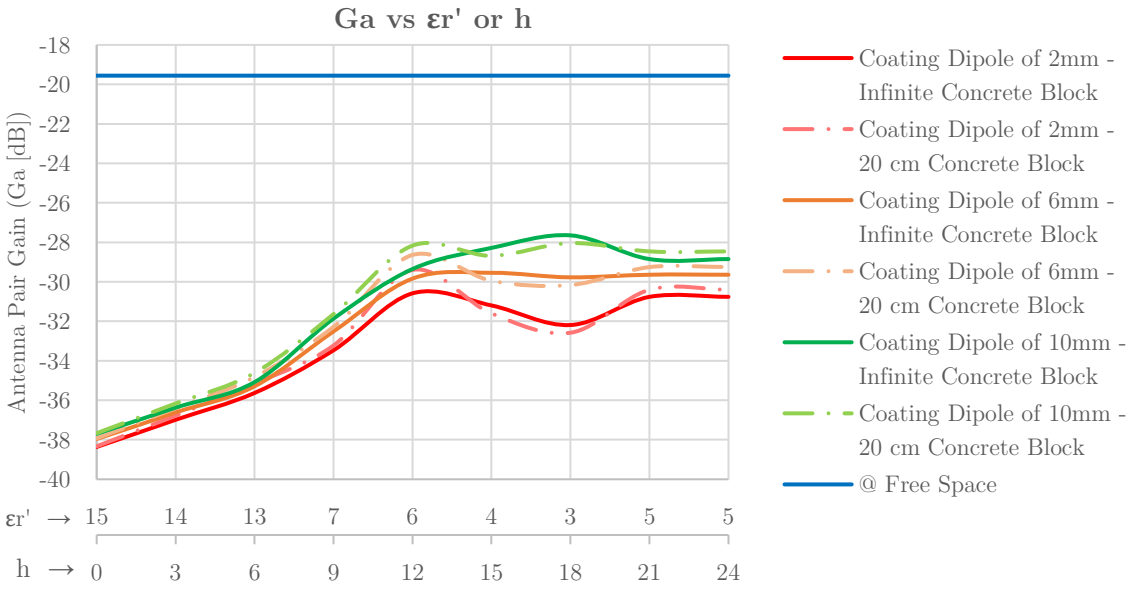

Figure 20: Comparison of infinite and finite models in terms of antenna pair gain during the drying process.

3.7 Chapter Conclusions

To conclude, the most important points seen throughout Chapter 3 are listed below:

1. The less the antenna is embedded in concrete, the higher the antenna pair gain. But in order to satisfy the specifications, H_2 = 6 cm is used (see Figure 12).
2. The ideal value for the length of the embedded dipole is the one that gives an antenna pair gain value as uniform as possible for the three concrete states. Accordingly, a value of L_2 = 6 cm is selected (see Figure 14). Although 5 cm diameter was the limitation in the specifications, 1 cm difference for this kind of application is not critical as it may be in applications where the antenna is implanted in the human body. In this case it is worth to have 1 cm longer antenna for a better link. However, if it is needed, miniaturizing the antenna from 6 to 5 cm would not be too difficult.
3. Adding a coating to the embedded dipole smoothes the transition of the signal between different mediums, giving a better result in terms of antenna pair gain. Nevertheless, a too thick coating can end up being a trouble in terms of antenna size (see Figure 17).
4. Working with infinite concrete for tests is not a poor approximation since the biggest difference from a finite concrete block is only 2 dB (see Figure 20). Hence, using an infinite medium is a good way to make reliable simulations at a low computational cost.

Chapter 4

Antenna Design and Experimental Results

4.1 Introduction

In this chapter, an antenna is designed in FEKO that will be feasible to replicate in reality; a dipole with a transmission line (to connect the antenna to the network analyzer). Comparing simulated and experimental results will allow us to corroborate some theoretical conclusions such as the value of the permittivity or the size of the appropriate antenna and in the case of deviations, to investigate the reasons and adjust them. For that purpose, the dipole is protected with FR4 plates so the antenna can be introduced in the concrete without contact with the medium. This can be designed creating a multilayer model, where each layer has a different permittivity assigned. The idea is shown in Figure 21.

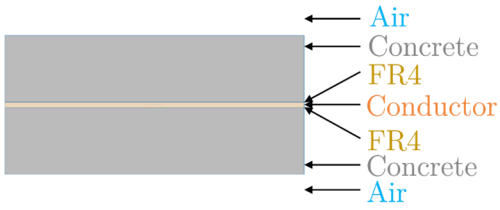

Figure 21: Horizontal view of the different layers and content.

4.2 Quarter-Wave Transformer

For the structure design, the first thing to do is create the dipole as defined in Section 3.4.1, L_2 = 6 cm. The width of the dipole arms and the gap between them are still to be defined; 6 mm and 2 mm are used for the simulations (Figure 22 (a)). Next, we need a transmission line so we can measure the antenna outside. To do so, we have to know the impedance at the dipole arms (Z_L) in order to define how should be the impedance of the transmission line we should add. Hence, we can spot already the need for impedance matching to maximize the power transfer or minimize signal reflection from the load. Consider that the following steps are made for a concrete in fresh state (for ε_r' = 14) and therefore it is expected that the resonance frequency will not be at 868 MHz but slightly lower – actually at 760 MHz.

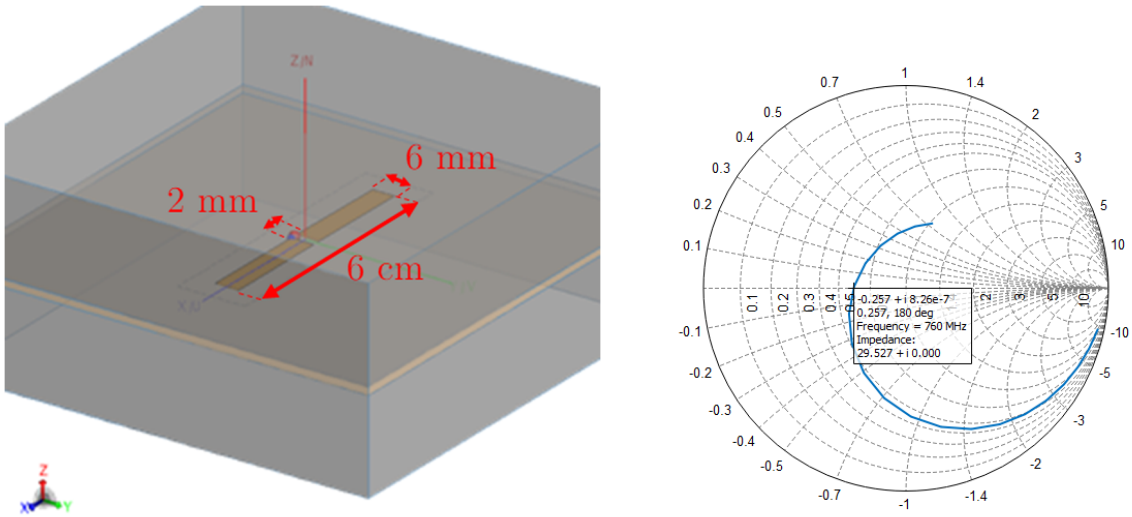

(a) Dipole arms

(b) Impedance for $\varepsilon_r' = 14$

Figure 22: Dipole arms and its resonance frequency.

As it is shown in Figure 22 (b), the input impedance of the antenna at the first resonance is $Z_L = 29.5\ \Omega$. The target is matching the load impedance to be 50 Ω so the quarter-wave transformer technique is used. A simple $\lambda/2$ line might also work (see Figure 23 - $|\rho| = 0.13$ (-17.5 dB)), however for our application, we are interested in a large bandwidth to follow the changes produced in the medium. Alternatively, using cascaded $\lambda/4$ lines, the bandwidth can be increased [18]. Besides, with $\lambda/4$ transitions the load is translated in half turn to the Smith Chart instead of a full turn, which gives more control when changing impedances.

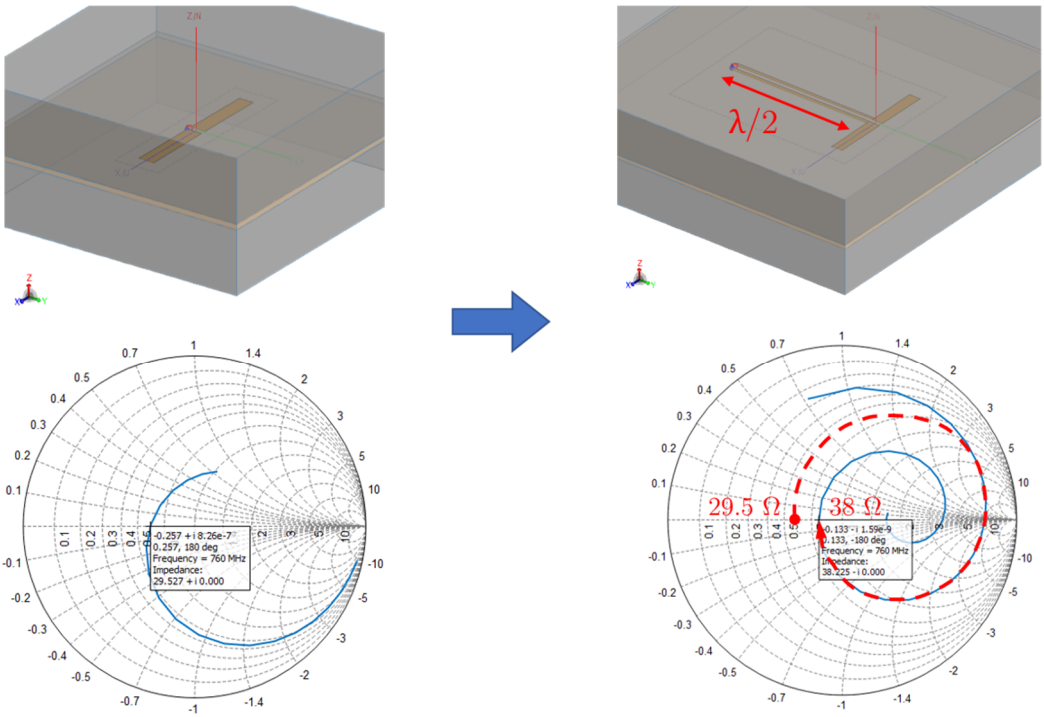

Figure 23: Half-wavelength transmission line effect at 760 MHz.

The input impedance of a transmission line of length L with characteristic impedance Z_0 and connected to a load with impedance Z_L is [18]

$$Z_{in}(L) = Z_0 \left[\frac{Z_L + jZ_0 \tan(\beta L)}{Z_0 + jZ_L \tan(\beta L)}\right], \tag{20}$$

where the propagation constant in the medium is $\beta = \frac{2\pi}{\lambda}$. An interesting thing happens when the length of the line is a quarter of a wavelength

$$Z_{in}\left(L = \frac{\lambda}{4}\right) = Z_0 \left[\frac{Z_L + jZ_0 \tan\left(\frac{2\pi}{\lambda}\frac{\lambda}{4}\right)}{Z_0 + jZ_L \tan\left(\frac{2\pi}{\lambda}\frac{\lambda}{4}\right)}\right] \quad \rightarrow \quad Z_{in}\left(L = \frac{\lambda}{4}\right) = \frac{{Z_0}^2}{Z_L}. \tag{21}$$

($\tan\left(\frac{2\pi}{\lambda}\frac{\lambda}{4}\right) \rightarrow \infty$ in both numerator and denominator)

It states that by using a quarter-wavelength of transmission line, the impedance of the load (Z_L) can be transformed via the above equation. However, we have to bear in mind that this is an embedded system where we have two different medias (FR4 + Concrete) that are going to impact on the transmission line length. So the first issue is to find the dielectric constant appropriate to work either in fresh state or in hardened state. For that, a simple scenario is built; a case, where we can isolate the effective dielectric constant (ε'_r). If we determine a random length for the transmission line – for instance 6 cm and we look at the frequency which the length is $\lambda/2$, the remaining unknown is ε'_r. That is to say, for a fresh state:

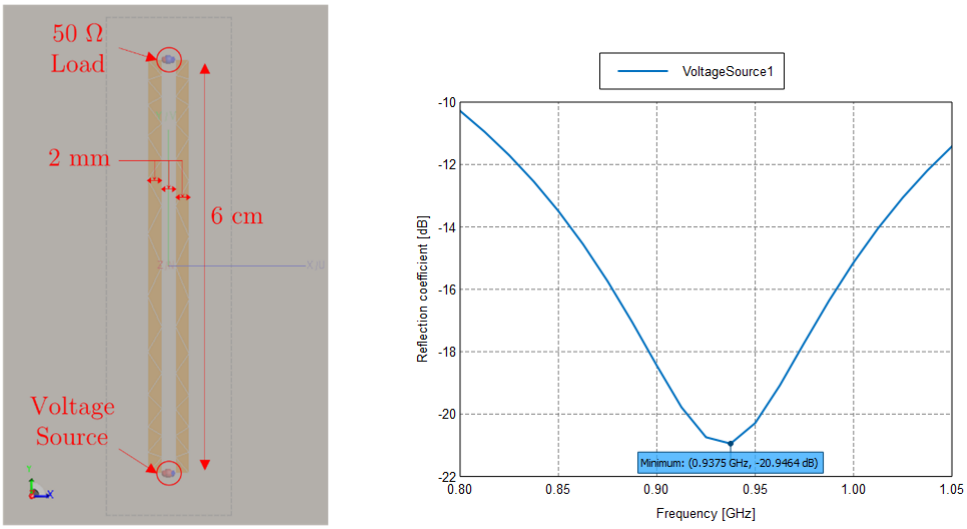

(a) Transmission Line Test (b) Reflection Coefficient

Figure 24: Transmission line to determine the dielectric constant.

$$L = 6\text{ cm} = \frac{\lambda}{2 \cdot \sqrt{\varepsilon'_r}} = \frac{c_0}{2 \cdot 0.93\text{ GHz} \cdot \sqrt{\varepsilon'_r}} \rightarrow \varepsilon'_{r\,fresh} = \left(\frac{c_0}{2 \cdot 0.93\text{ GHz} \cdot 6\text{ cm}}\right)^2 = 7.2 \tag{22}$$

Same scenario but for a hardened state is

$$L = 6\ \text{cm} = \frac{\lambda}{2 \cdot \sqrt{\varepsilon_r'}} = \frac{c_0}{2 \cdot 1.13\ \text{GHz} \cdot \sqrt{\varepsilon_r'}} \rightarrow \varepsilon_{r_{\text{hardened}}}' = \left(\frac{c_0}{2 \cdot 1.13\ \text{GHz} \cdot 6\ \text{cm}}\right)^2 = 4.9\,. \tag{23}$$

Then, as the idea is be able to work in any concrete state, a correct value of dielectric constant can be whatever between the range [4.9 – 7.2]. With this, we already determine the length of our quarter-wavelength transmission line; as start-up and to get an idea of how its length will be, we can average the extreme cases, this is $\varepsilon_r' = 6.05$:

$$L_{\frac{\lambda}{4}\text{TL}} = \frac{\lambda}{4 \cdot \sqrt{\varepsilon_r'}} = \frac{c_0}{4 \cdot 868\ \text{MHz} \cdot \sqrt{6.05}} = 3.5\ \text{cm} \tag{24}$$

Now, we want to match a load with impedance $Z_L = 29.5\,\Omega$ to be 50 Ω using the quarter-wave transformer. The problem is to determine Z_0 (the characteristic impedance of our quarter-wavelength transmission line) such that the 29.5 Ω load is matched to 50 Ω. Applying equation (21), the problem is simple

$$50\ \Omega = \frac{{Z_0}^2}{29.5\ \Omega} \quad \rightarrow \quad Z_0 = \sqrt{50\ \Omega \cdot 29.5\ \Omega} = 38.4\ \Omega \tag{25}$$

Hence, by using a transmission line with a characteristic impedance of 38.4 Ω, the 29.5 Ω load is matched to 50 Ω. Hence, if a transmitter has an impedance of 50 Ω and is trying to deliver power to the load (antenna), no power will be reflected back to the transmitter. Nevertheless, to achieve a 38.4 Ω transmission line, it needs to be very wide (2.4 cm) and this can carry out a distortion of our dipole antenna and in consequence, in the radiation pattern. As we see in Figure 25 at 760 MHz, the maximum is not always in the Z direction.

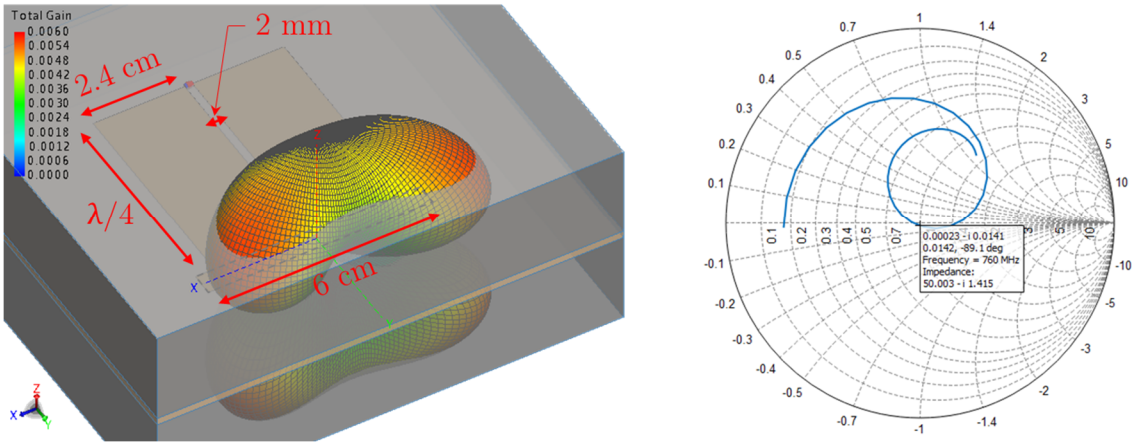

Figure 25: Effect of characteristic impedance on transmission line width at 760 MHz.

Imagine that we have a lossless line, the equation for characteristic impedance reduces to $Z_0 = \sqrt{L/C}$ where L and C are the inductance and capacitance per unit length respectively. Then, when strip width↓, L↑, Z_0↑. For that reason, it is recommended to start with a thin

track and make the needed quarter wave transformations until reaching the desired width. So we start by using a narrow transmission line, for instance, a quarter-wave transmission line of 2 mm wide. A $\frac{\lambda}{4}$ section of transmission line is equivalent to half a turn around the Smith Chart so now we have an impedance of 348.7 Ω.

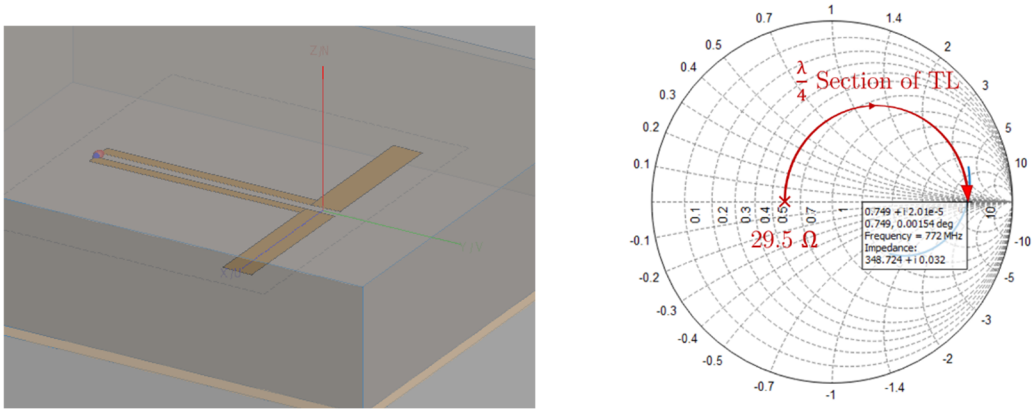

(a) Dipole arms with a λ/4 section (b) Impedance for $\varepsilon_r' = 14$

Figure 26: Dipole arms with a **λ**/4 section and its resonance frequency.

This is a transmission line of 101.4 Ω. From (21)

$$Z_0 = \sqrt{Z_L \cdot Z_{in}} = \sqrt{29.5\,\Omega \cdot 348.7\,\Omega} = 101.4\,\Omega\,. \tag{26}$$

Now is time to add a second $\frac{\lambda}{4}$ section of transmission line so we can reduce the 348.7 Ω of before without alter the radiation pattern.

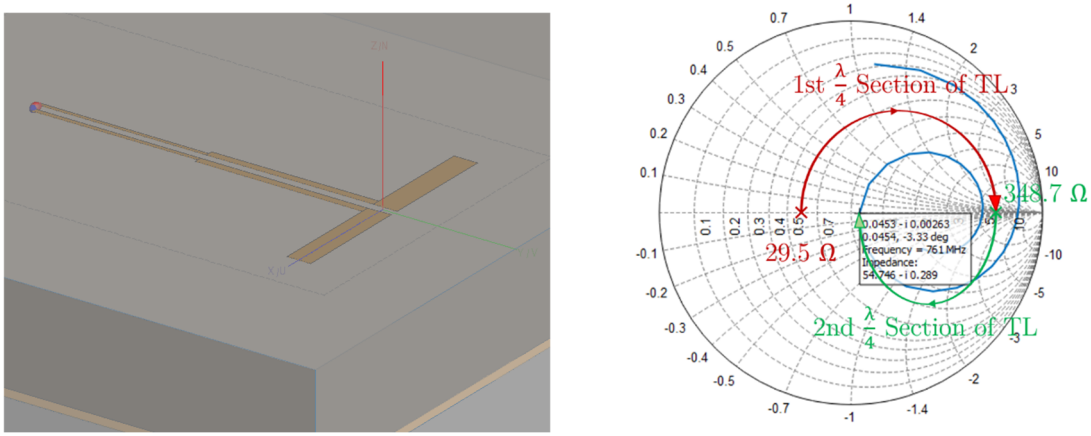

(a) Dipole arms with two λ/4 sections (b) Impedance for $\varepsilon_r' = 14$

Figure 27: Dipole arms with two **λ**/4 sections and its resonance frequency.

As we can see in Figure 27 (b), the value of Z_{in} now is 54.7 Ω. Then, similarly to (26), we can find out the characteristic impedance of the second transmission line

$$Z_0 = \sqrt{Z_L \cdot Z_{in}} = \sqrt{348.7\ \Omega \cdot 54.7\ \Omega} = 138.1\ \Omega\,. \tag{27}$$

Z_{in} = 54.7 Ω is a value very close to the 50 Ω we were looking for, however, the last section of transmission line is 138.1 Ω ≠ 50 Ω. As it is not 50 Ω, another section of transmission line of 50 Ω should be added to ensure that the transition is made correctly. For this we do the following calculus. From (20), if new Z_L = 54.7 Ω and I want a characteristic impedance Z_0 = 50 Ω, considering a section of 2 cm, I have to expect a Z_{in} = 54 Ω approximately

$$Z_{in}(L = 2\ \text{cm}) = 50\ \Omega \left[\frac{54.7\ \Omega + j50\ \Omega\ \tan\left(\frac{2\pi}{\lambda} 0.02\ \text{m}\right)}{50\ \Omega + j54.7\ \Omega\ \tan\left(\frac{2\pi}{\lambda} 0.02\ \text{m}\right)}\right] = 54\ \Omega\,. \tag{28}$$

To reach Z_0 = 50 Ω in the final section, a strip with 12 mm width is introduced as shown in Figure 28. The thickness of the transmission line is already something we do not care much about because we are no longer so close to the dipole arms and therefore it should not affect the radiation pattern. This is confirmed in Figure 30.

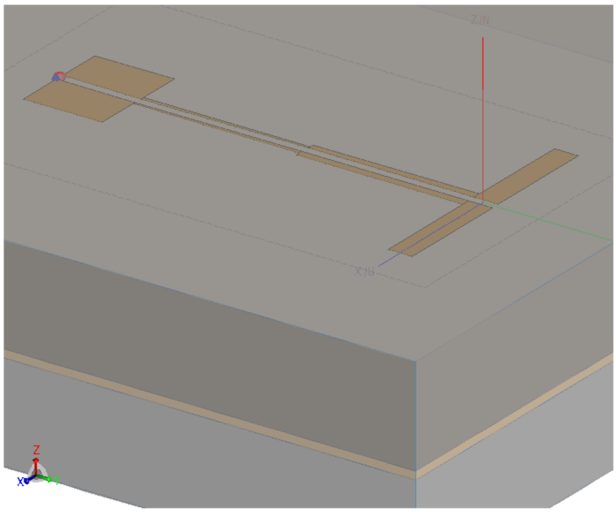

(a) Dipole arms with two λ/4 and 50 Ω sections

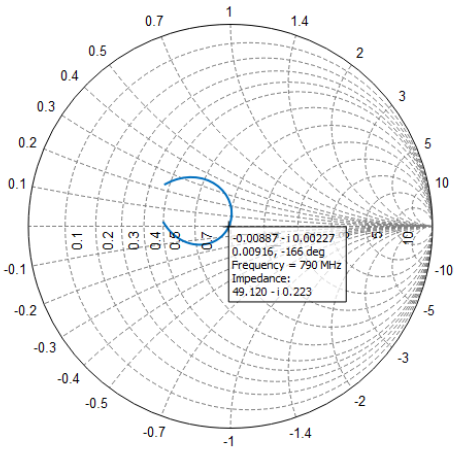

(b) Impedance for $\varepsilon_r' = 14$

Figure 28: Dipole arms with two **λ**/4 sections ending up with a 50 **Ω** transmission line and its resonance frequency.

To summarize, the dimensions of the dipole and its transmission line as well as the impedance values along each section are gathered in Figure 29 (a) and (b) respectively.

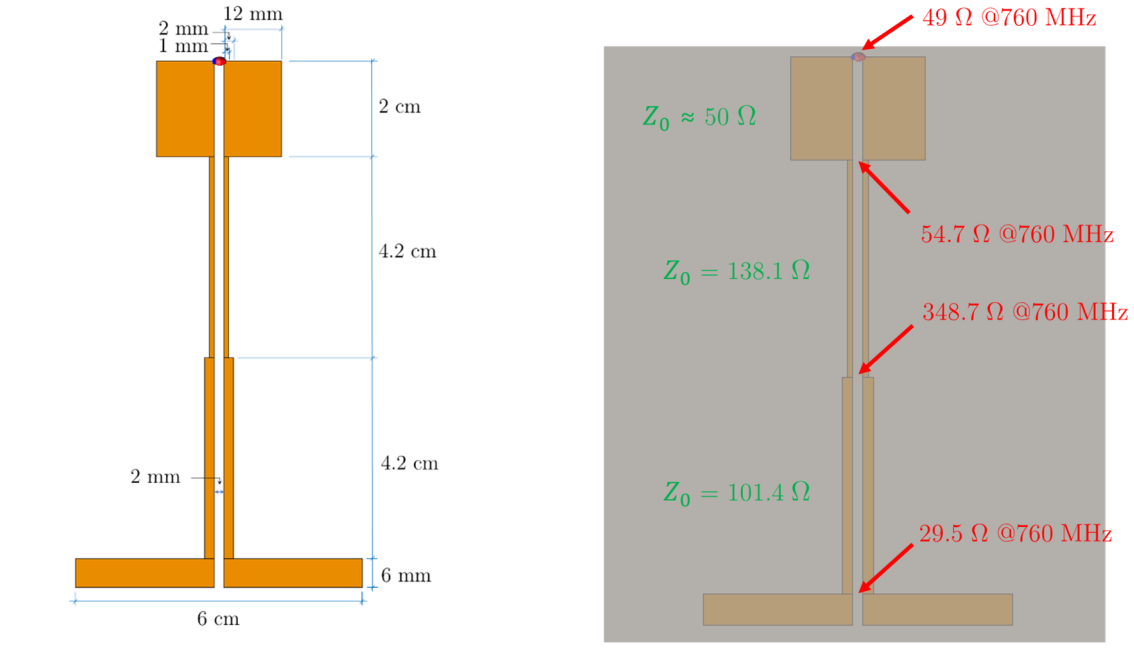

(a) Dipole and Transmission Line Sizes (b) Impedance Values

Figure 29: Summary of the dipole and its transmission line in terms of size and impedances.

4.2.1 Simulation results

To ensure that the antenna transmits with a uniform radiation pattern and that the last widest section does not distort the diagram, Figure 30 shows the far fields request in concrete and free space. Note that the 3D pattern belongs to the typical shape of a half-wave dipole.

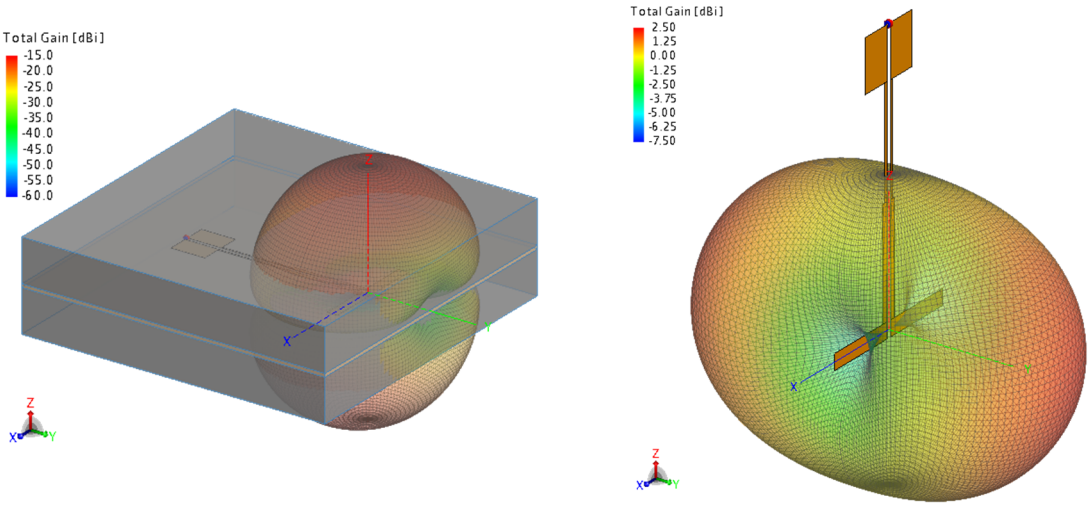

(a) Radiation Pattern in Concrete (b) Radiation Pattern in Free Space

Figure 30: Radiation pattern in concrete and free space – results at 0.760 GHz.

With this structure, for each of the concrete states (different permittivities) the reflection coefficient is ≈ -11.5 dB for the worst case (fresh state) at 868 MHz. We can also see that as the concrete dries and loses water, the working frequency shifts to the right. Hence, we have to try to be in the middle of the three states. It is a complex process since the fact of being in a medium with changing permittivity causes the resonance frequency to move easily.

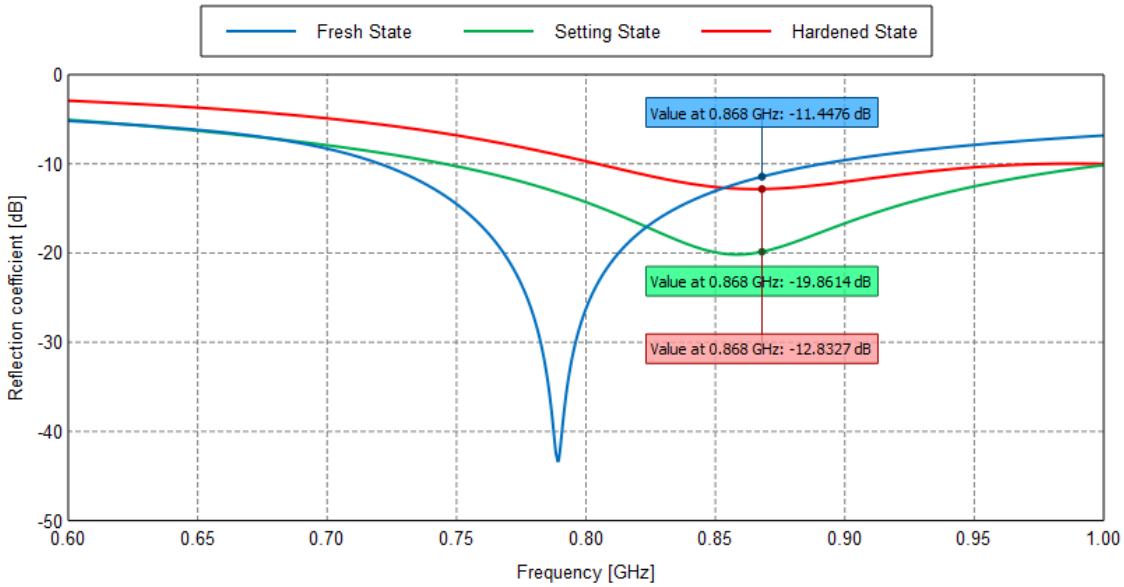

Figure 31: Reflection coefficient for the prototype antenna during the drying process.

Nevertheless, the whole design is made with multilayer and with the transmission lines completely inside the concrete. And therefore, this does not correspond to what would have to be mounted for the measurement. With all the lessons learnt from the multilayer design, a model with finite concrete and finite substrates should be designed as close as possible to how it will be measured. The multilayer model, even it does not correspond to something real, it serves to adjust the impedances of the lines in a simpler way and at a not so high computational cost. However, changing to a finite model will have an impact in the design, so the antenna will have to be adjusted (lengths, lines widths, etc.) again to work properly.

4.2.2 Quarter-wave transformer: finite model

The next step then, is to test the same antenna but with a finite cube (10 x 10 cm) where part of the transmission line protrudes so that the antenna can be connected to the VNA. Comparing the result in Figure 32 (c) against the one obtained in Figure 31, it seems that the frequency has shifted a bit to the left, however, it still follows the same pattern as before; when the concrete dries, the frequency increases, that is good.

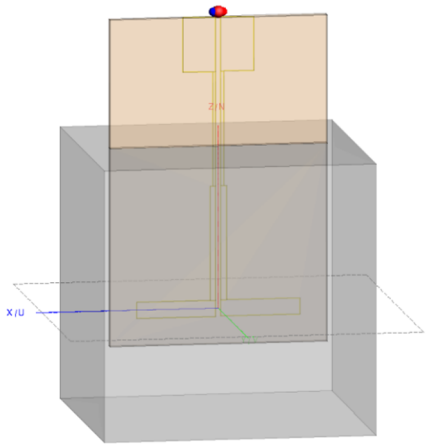

(a) Antenna with Finite Cube

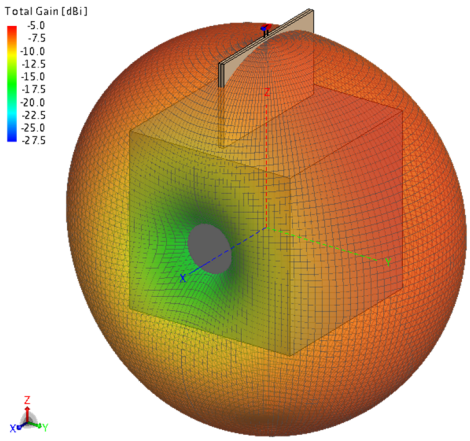

(b) Radiation Pattern @ 0.73 GHz

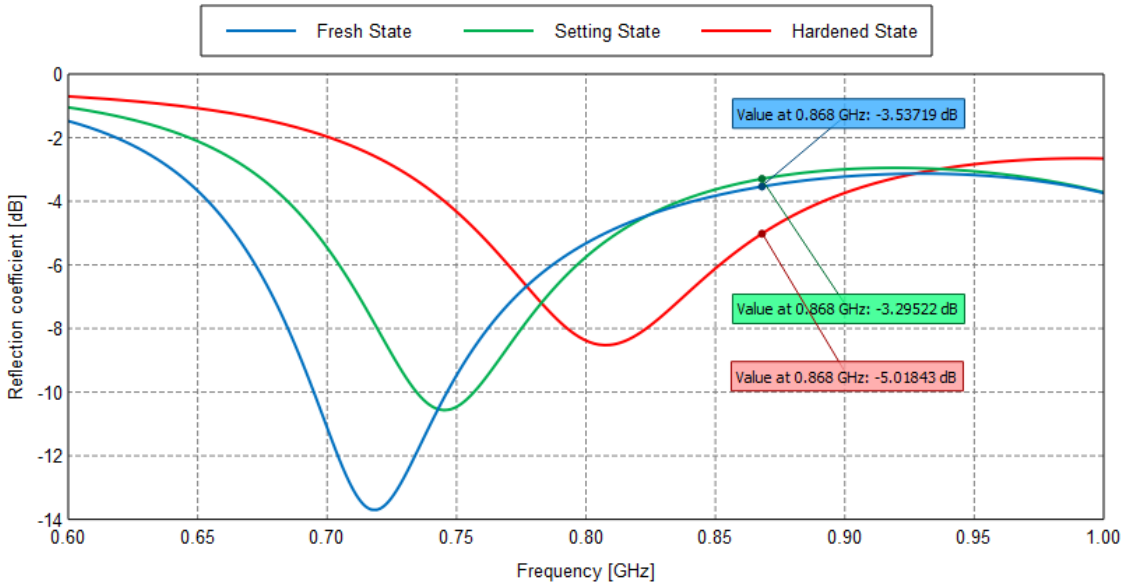

(c) Reflection Coefficient

Figure 32: Antenna for a finite cube of concrete.

Note that by changing from the infinite to the finite model, we have lost the matching to 868 MHz quite a bit because the whole set of operating frequencies has shifted to lower frequencies. Therefore, the lines will have to be adjusted again until a proper matching is achieved, but first, we must add some important details in the model.

4.3 Antenna Refinements: Feeding Point and Container

An adjustment to consider is at the feeding point. It should be noted that the line ends with 12 mm width and that the connector is a coaxial whose external diameter is approximately

4 mm [21]. Therefore, it is necessary to make a transition from 12 to 4 mm because if the line is wider than 4 mm the strip will short-circuit the ground with the feeding point of the connector (see Figures 33 (a), (b)). All this without losing too much the 50 Ω (matching) of that line. Figure 33 shows how the feeding will be done, at least initially, with the aim of having something to manufacture and measure that tells us how far we are from reality. Moreover, in the real scenario the connector will not be floating as we had it until now in the models, so one of the two plates of FR4 has to be a little shorter to put (and weld) the feeding point of the connector (see Figure 33 (c)).

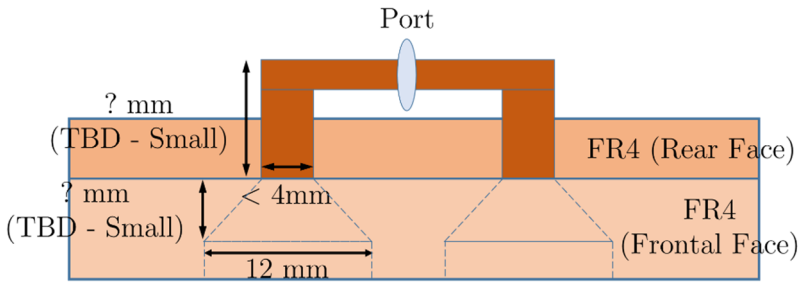

(a) Transition in the Feeding Point – Draft

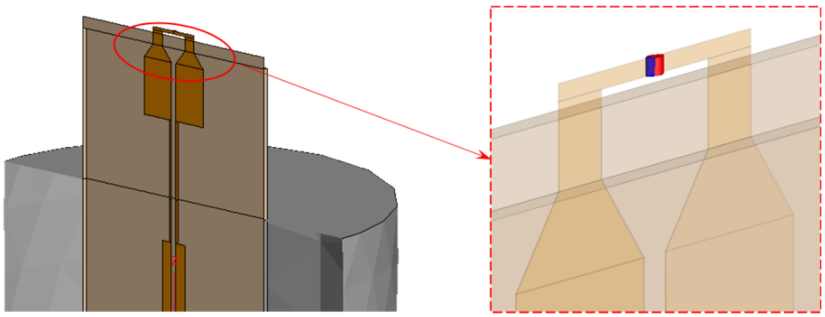

(b) Transition in the Feeding Point – FEKO

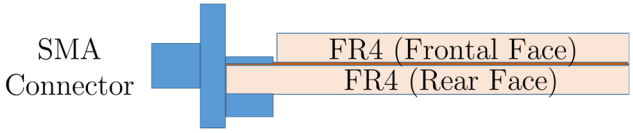

(c) Detail in the Feeding Point – Horitzontal View

Figure 33: Radiation pattern in concrete and free space.

4.3.1 Simulation results

Note that besides that, the concrete cube has to be modified as well to have the shape of the real container to be used in the experiment. In the laboratory we have a cylindrical tupper with a diameter of 14 cm and a height of 9.5 cm that could suit for the experiment. Considering all this, Figure 34 shows the result so far.

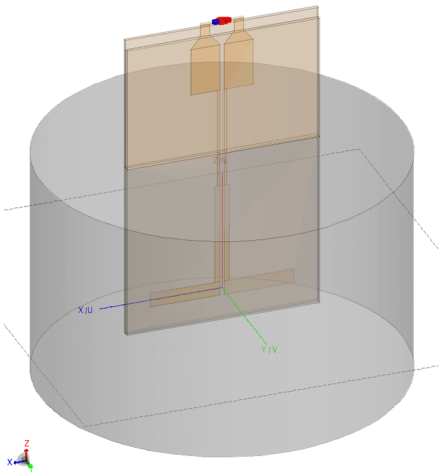

(a) Antenna with Real Container

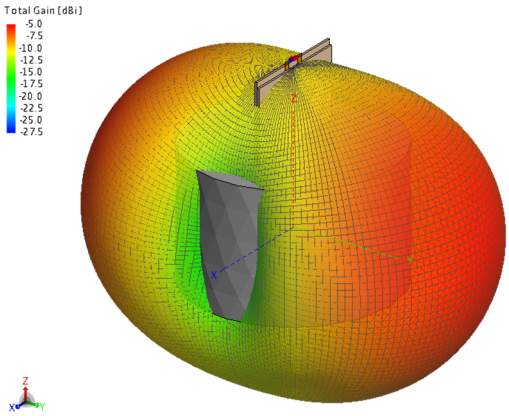

(b) Radiation Pattern @ 0.7 GHz

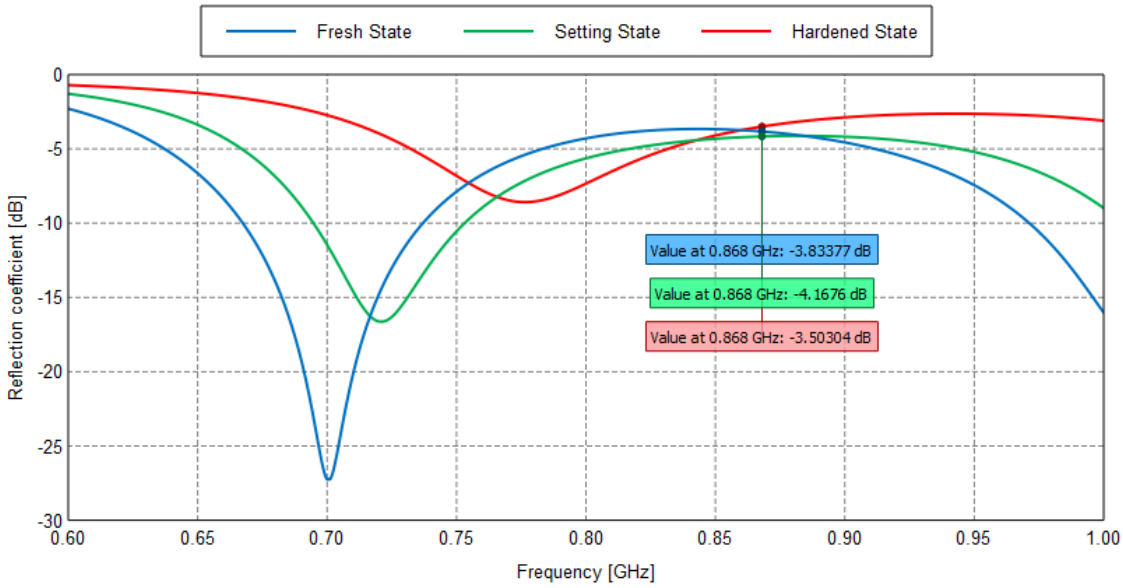

(c) Reflection Coefficient

Figure 34: Results after the transition and changing the antenna container.

As we can observe in Figure 34 (c), the trend is good; in the fresh state the resonance is at slightly lower frequencies and as the permittivity of the concrete decreases the frequency is higher. However, we are about 100 MHz to the left of what we would like (868 MHz).

4.4 Antenna Refinements: Resize of Transmission Lines

At this point, the transmission lines must be modified to better adjust the matching levels (widths, lengths, etc.). In our case, the lengths of the strips and especially the width of the

last 50 Ω section had to be modified – see Figure 34 (a) against Figure 35 (a). With this adjustment, we get the antenna to work in the band of interest, moving the working frequencies of Figure 34 (c) to higher frequencies. The dimensions are detailed in Annex B.

4.4.1 Simulation results

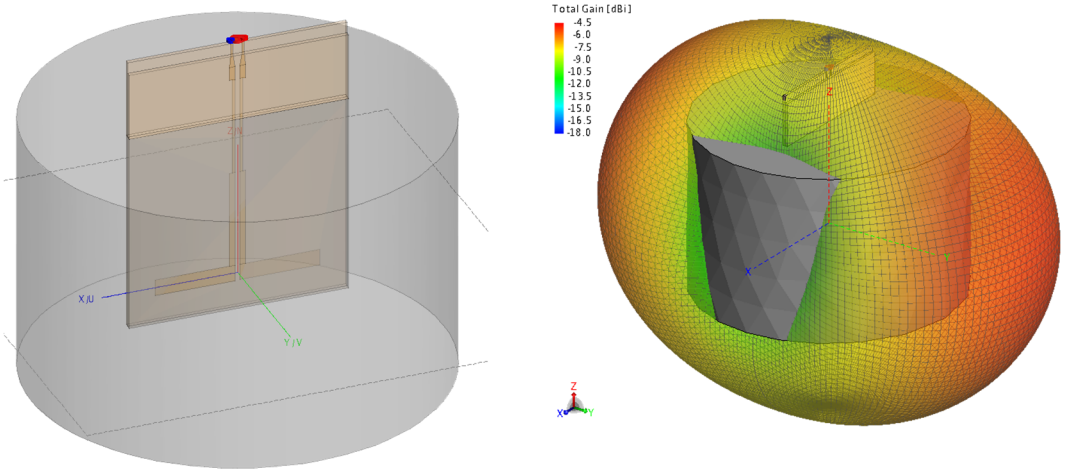

(a) Readjusted antenna

(b) Radiation Pattern @ 0.815 GHz

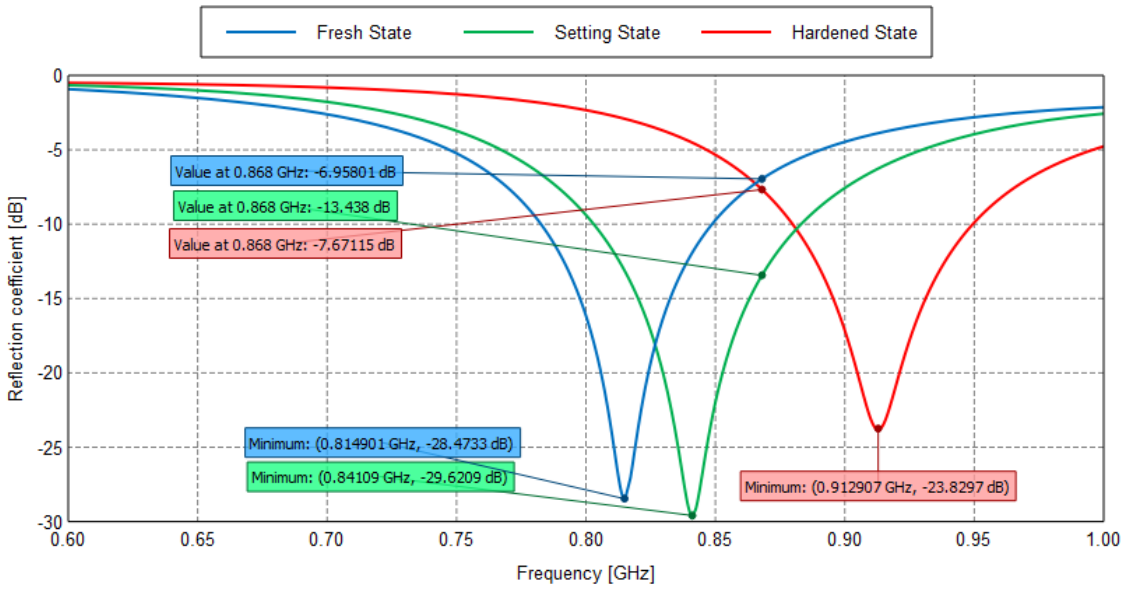

(c) Reflection Coefficient

Figure 35: Results after readjust the antenna for a proper matching.

As it can be seen in Figure 35 (c), the antenna has been found to work well for all three states of the concrete. The variation in the drying process is only about 100 MHz (between fresh and hardened state) and at the same time, it covers the 810 – 910 MHz range. And therefore, it covers our frequency of interest, the 868 MHz. Moreover, in the band the worst case is less than -6 dB (25% maximum power loss by reflection). Which indicates an improvement over previous models. Regarding the radiation pattern, we can say that it is still quite uniform, without secondary lobes and according to what is expected for a dipole radiation pattern. Having fulfilled the target, we send the model to be fabricated in order to make real measurements and contrast them with the simulated ones.

4.5 Real Measurements

In this Section, the results obtained after the fabrication of the antenna of Figure 35 (a) are shown. In Figure 36, we can compare the fabricated model with the one created in FEKO, and as we can observe, it is an exact replica of what was designed.

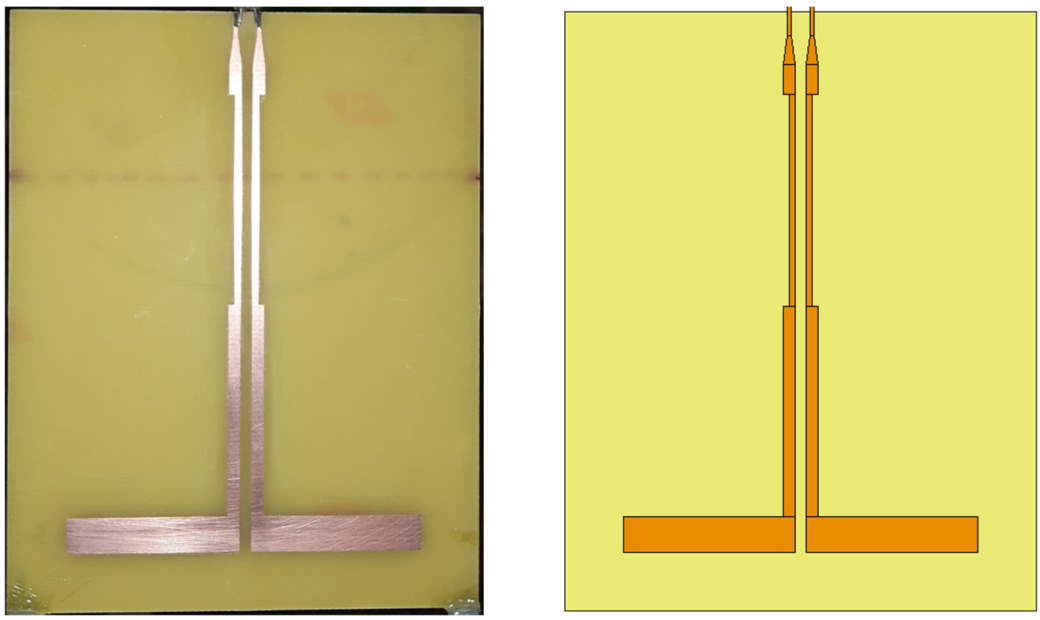

(a) Fabricated antenna (b) Designed antenna

Figure 36: Comparison of the fabricated antenna with the one designed in FEKO.

The first challenge in a practical experiment is to set up the stage. Although it may not seem like it, it is something tedious that is no often took into account and requires time to be as stable as possible. In our case, we work with concrete so the working area must be well protected. Besides, the antenna is inserted vertically and the coaxial cables are quite rigid, so they tend to bend (doing some squeeze). That is why we will have to make use of guides and holders to avoid forcing anything and get a confident and resistant scenario.

4.5.1 Measurements with a single FR4 plate in free space

First of all, to exclude possible deviations by the concrete, the antenna is measured with a single FR4 plate and without interaction with the concrete. The scenario is shown in Figure 37.

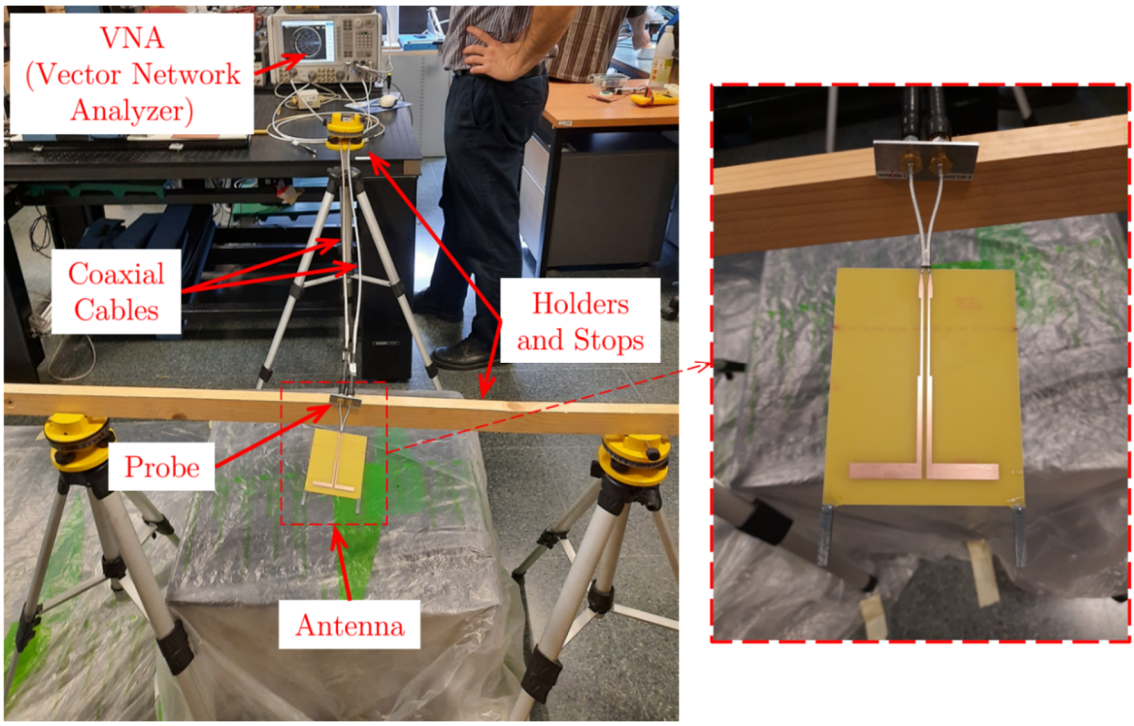

Figure 37: Scenario to measure the antenna in free space.

For the antenna measurements, we have used the N5242A PNA-X Network Analyzer from Agilent Technologies [22]. This instrument will measure the S-parameters of our antenna. In order to obtain adequate measurements, there are a couple of important steps to be addressed; calibrate the network analyzer with the coaxial cables that we will use and then, include the effects that the probe introduces in the measurements.

The network analyzer must be calibrated before any S-parameter measurements of the device under test are performed to ensure that the effects of cables, connectors, etc., are nulled out. Components of the measurement setup, such as interconnecting cables and adapters, introduce variations in magnitude and phase that can mask the actual response of the device under test. Calibration is then a very useful process to improve measurement accuracy as it removes one or more of the systematics errors. A good calibration is dependent on the quality of the calibration kit standard devices, the care with which they are maintained, and the correctness and repeatability of the device connections. Hence, it is important to be careful not to cause damage to the calibration kits as these can be very costly to replace. For calibration instructions, more detailed information is available in the Agilent Operating and Programming Manual [22].

On the other hand, a probe had to be used to connect the antenna to the network analyzer because as we can see in Figure 29 (a), the separation distance between transmission lines is very small (2 mm). By using the probe, we are adding an extra element in our design that we did not consider, however, the probe is designed (and labeled) so that its presence is automatically compensated by the network analyzer when entering its values. And therefore, we can connect to the antenna avoiding not required connectors in the final solution. Once the measurement setup is ready, we can start making measures. To do so, a technique called differential measurements has been applied.

4.5.1.1 Differential measurements

Making differential measurements means measuring the difference between two ports [23]. The reason we do this is because if we take measurements from only one port, we would have an unpredictable and unwanted result that is introduced by the position and length of the coaxial cable. And this is related to the currents that circulate in the external mesh of the cables. In the case of having a dipole with only one port (one coaxial cable), we would have the positive currents traveling inside the cable (I_1 – Figure 38) but also negative currents that would escape, traveling through the mesh of the cable (I_3 – Figure 38). The problem that would occur is that some of the negative currents traveling through the mesh would bounce back when arriving to the dipole ($I_2 - I_3$ – Figure 38), producing a variable, undesired and uncontrollable interference, depending on the position of the cable affecting then on radiated fields and input impedance. This current flow can be seen in Figure 38.

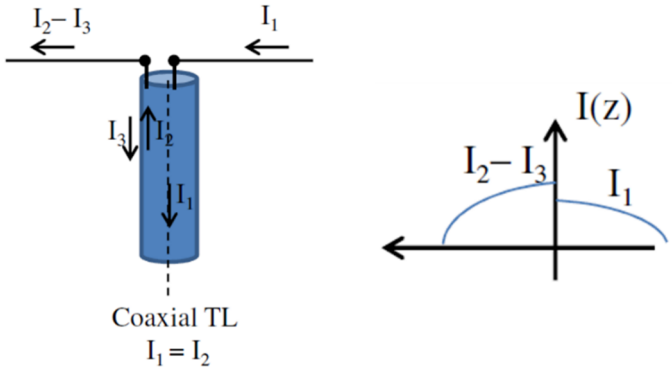

Figure 38: Differential measurements – Currents through the coaxial.

The solution to this problem is using two cables for the measurements; one for the positive currents and the other one for the negative ones. By doing this, we will have to bear in mind that the coaxial where the positive current travels will have to be powered with V/2 and the coaxial for the negative currents will be powered at -V/2. Then we make sure that the positive current is equal to the negative current, but with opposite sign. This is done automatically with the network analyzer. It is important to consider that since the differential measurements are taken with two 50 Ω coaxial cables, the results will have to be displayed over a 100 Ω impedance. Thus, all of the next comparisons refer to 100 Ω.

4.5.1.2 Measure and simulation results

As introduced, the first test is to compare results when using a single FR4 plate and without interaction with the concrete. Note that for this test it is not convenient to suspend the antenna for a long time by its own weight because as you can see in Figure 37, the weld spot at the feed point is very small and therefore very delicate. Another thing to consider is that the dielectric constant of FR4 can vary a lot depending on the manufacturer; it may start with 4.6 at low frequencies and decrease up to 4 for frequencies beyond 1 GHz [24]. The same occurs with the loss tangent. The value for the dielectric properties of FR4 used in the simulation are $\varepsilon r = 4$ and $\tan \delta = 0.03$. The result is shown in Figure 39.

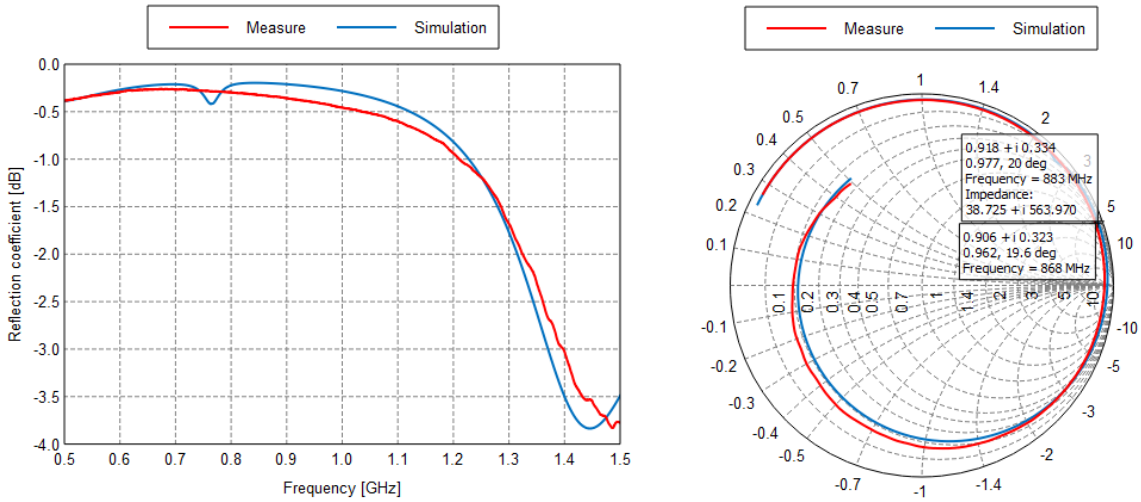

Figure 39: Reflection coefficient and impedance for scenario in Figure 37 – Measure and Simulation (reference impedance: 100 Ω).

As expected, the resonance frequency for the antenna in free space is out of our range of interest since the size of the current antenna is not designed to work in free space but in concrete (see equation (5)) and the transmission lines are also adjusted taking into account two different media, FR4 and concrete. In Figure 39, we can see that simulation and real result have a very similar trend although slightly shifted in frequency. This can be due to several reasons (meshing, connectors, method, FR4 properties, etc.) but the most likely is that the difference is due to the feeding point. As it has been said, it is a sensitive point and it is easy that with something that the simulation does not take into account, it makes the result vary.

4.5.2 Measurements with both FR4 plates in free space

Before immersing the antenna, we make a last measurement comparing again the simulated and the real result obtained. This time, with the antenna sealed by the two plates of FR4

but not yet inserted in concrete. This measurement will give us an idea of how the antenna behaves when it is between two FR4 plates and in turn, compare how it changes with respect to the results obtained in Section 4.5.1.2. Figure 40 shows the two plates of FR4, where we can see a red dotted line that indicates the depth at which the antenna should be (H_2 = 6 cm). Using stoppers will help to avoid the antenna to be in direct contact with the base of the recipient and at the same time, avoid the antenna to be more than 6 cm deep.

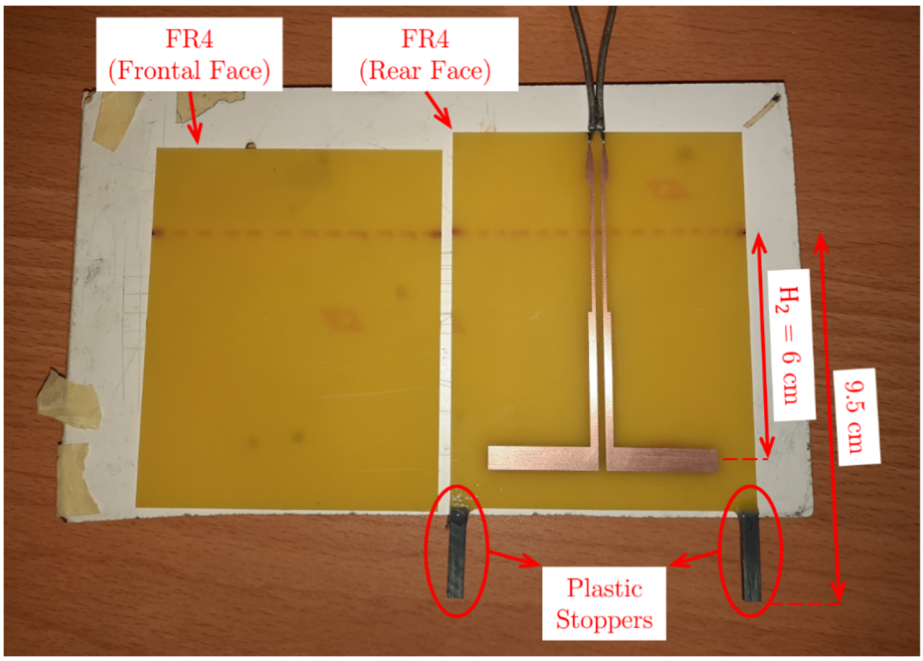

Figure 40: Disassembled antenna.

To seal the antenna, silicone is used, covering the whole contour of the FR4 plates to prevent water from entering. It is important not to cover the feed point with silicone because this could spoil the result. Also, by using some heavy material, we prevent air from remaining inside the FR4 plates and we proceed with the sealing. The result can be seen in Figure 41.

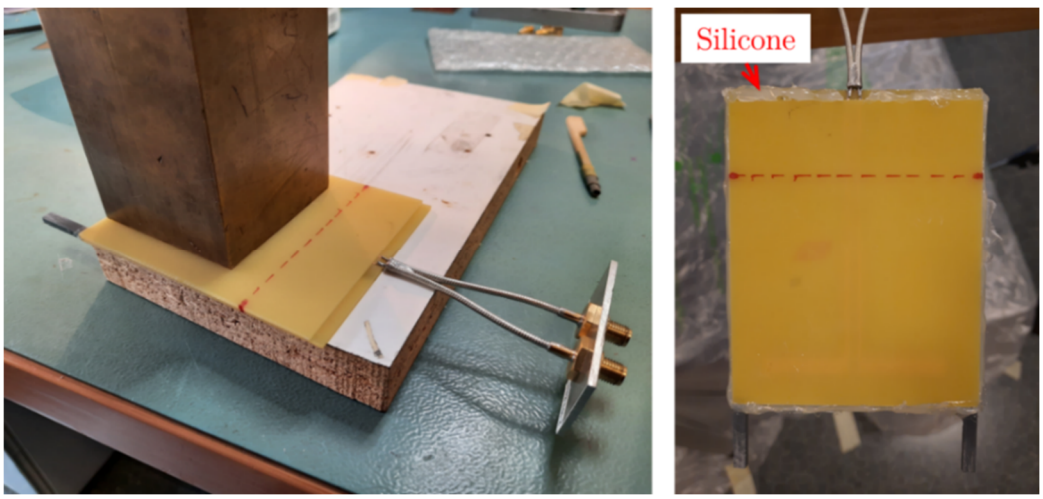

Figure 41: Antenna sealing process.

Again, the scenario is pretty similar to the one in Figure 37. The new measurement scenario can be seen in Figure 42.

Figure 42: Scenario to measure the antenna in free space with both FR4 plates sealed.

4.5.2.1 Measure and simulation results

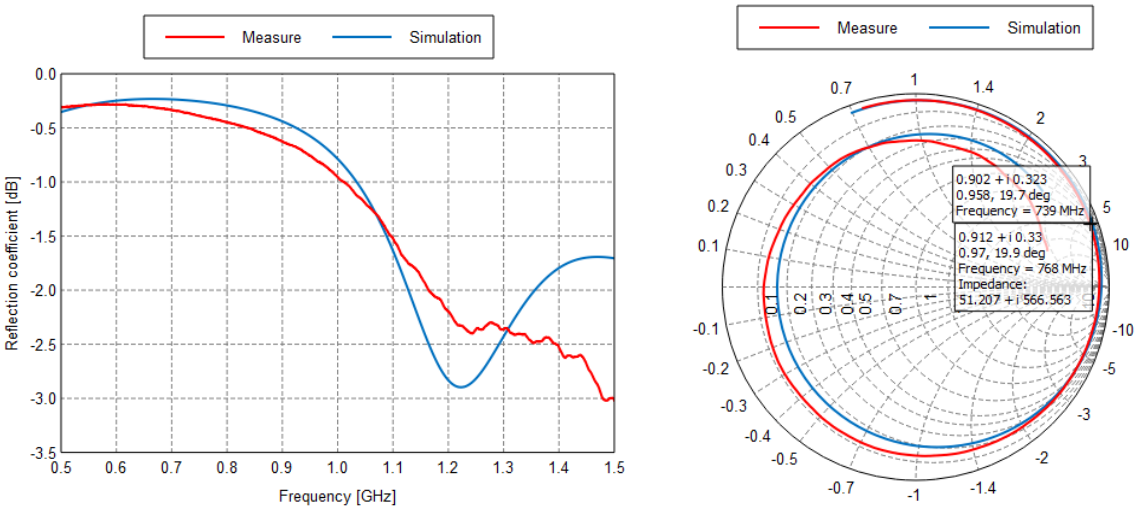

Figure 43: Reflection coefficient and impedance for scenario in Figure 42 – Measure and Simulation (reference impedance: 100 Ω).

Similarly to Figure 39, the theoretical and experimental result has a very high reflection coefficient (≈ -3 dB) because its operating frequency is at higher frequencies, outside our range of interest and possibly also because we have changed the reference impedance from 50 to 100 Ω. Although at first glance they look like different traces, the biggest difference between curves is just ≈ 1 dB. The main difference from the previous measure is that the result has generally moved a little bit at lower frequencies in the direction we want. And this makes sense because as the model is more similar to what we really want to have, it should give a result closer to our frequency of interest. Therefore, when the antenna is inside the concrete we expect to see a much lower reflection coefficient and hence we can make a better analysis. Anyway, so far we have seen that the real and simulated result is quite similar and therefore we can have the focus on the measures with concrete.

4.5.3 Measurements with the antenna in cement

Whilst the silicone dries, we proceed to create the compound. For this practical test, we create cement instead of concrete; a handful of stone or sand will change our permittivity little since the differential factor is the water content.

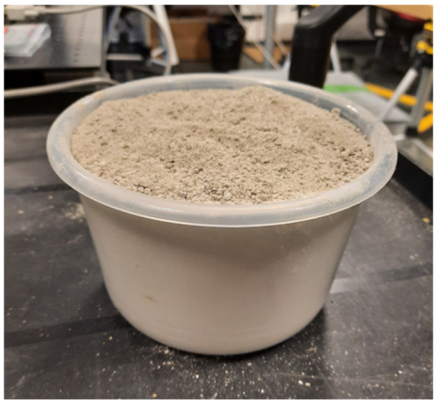

(a) Cement Portion

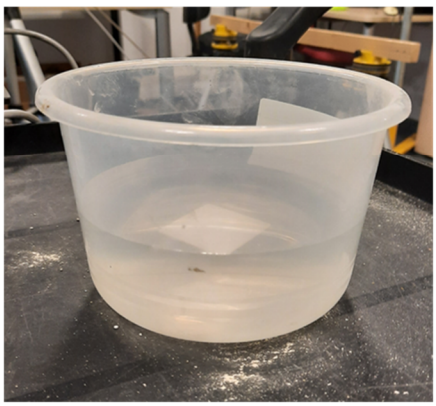

(b) Water Portion

(c) Ingredients Mixing

Figure 44: Cement creation process.

The water-cement ratio (w/c) is the ratio of the weight of water to the weight of cement used in a concrete mix [25]. For this experiment, we based on the capacity of the recipient in Figure 44. For reference, this recipient volume is 1.1 L and considering that 150 ml water ≈ 100 g cement. Then, the exact amounts were:

- **Water**: ½ x recipient of water (Figure 44 (b)) (550 ml = 550 g).
- **Cement**: 1 x recipient of cement (Figure 44 (a)) (733.3 g) + ¼ additional (183.3 g).

This is a w/c = 0.6 approximately (550 g water/916.6 g cement). The extra portion of a quarter of cement was due to the mixture being too watery. With that extra cement we managed to speed up the drying process and also get closer to our study reference of w/c = 0.45 (see Figure 7) and hence obtain a fairer comparison.

With the cement ready, we fill the recipient and then we introduce the antenna. Before starting measurements, it is important to remove the air from inside the container by compressing and uncompressing it a bit as shown in Figure 45.

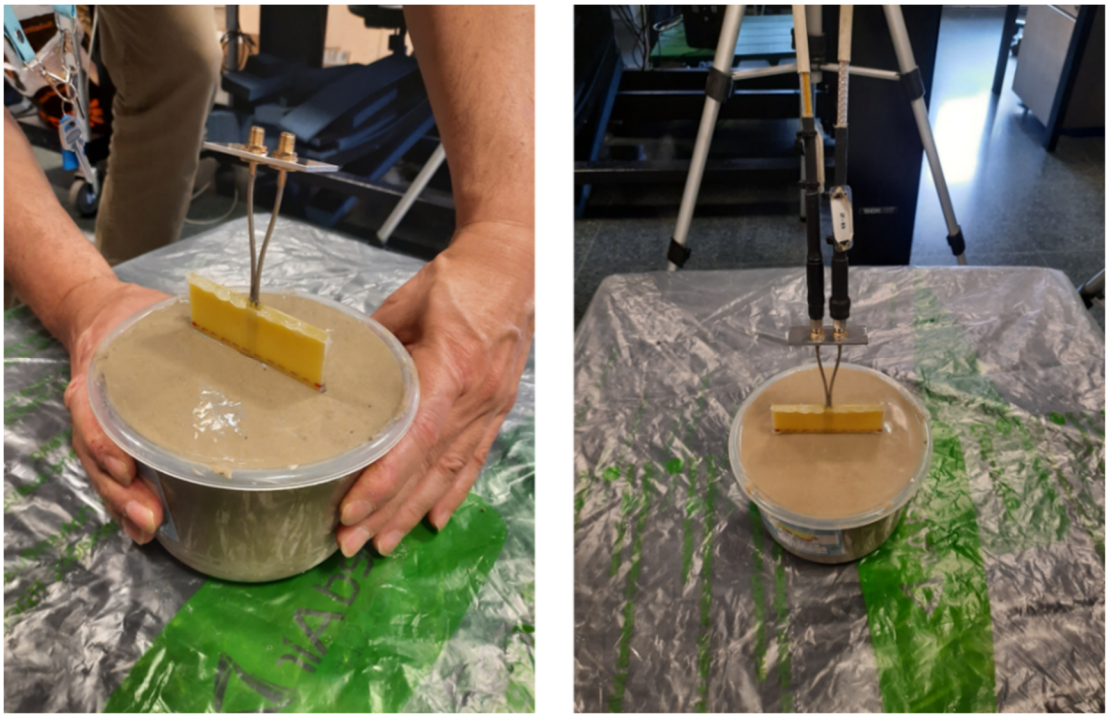

Figure 45: Antenna embedded in cement.

Once the antenna is embedded in the cement we have to make the first measurement. From then on, every hour a measurement is captured manually to see the progress during the drying process. The full scenario till now is shown in Figure 46.

Figure 46: Scenario to measure the antenna in cement.

In Figure 47, we can see the state of the cement after 9 hours drying. As it is a plastic container, it seems that the water only evaporates from the top and therefore that layer of water remains on the surface. Also, after 9 hours the cement was still quite fresh, perhaps because of the difficulty of evaporating the water or due to the excess of water.

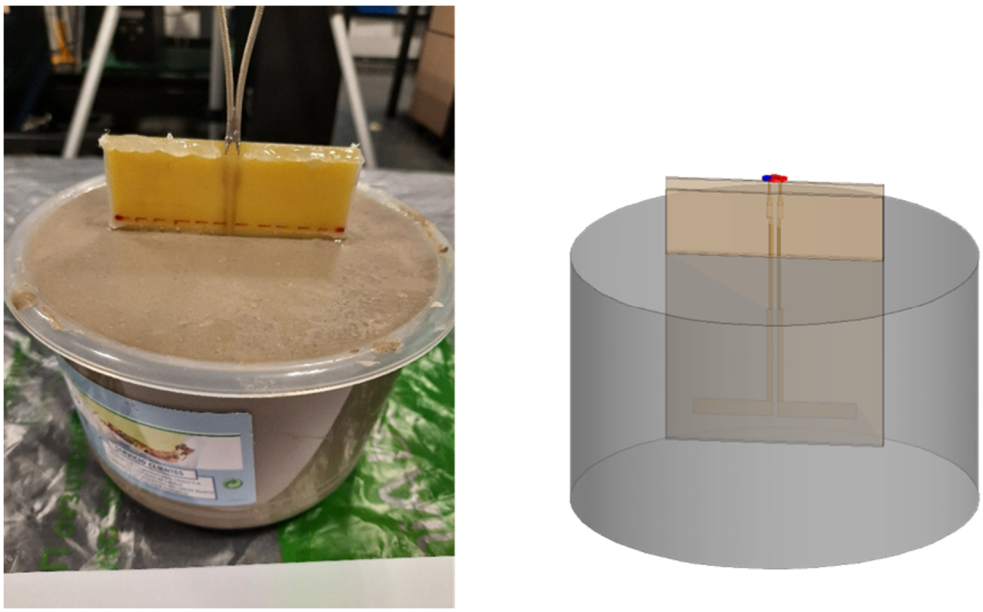

Figure 47: Antenna embedded in cement after 9 h together with FEKO design for comparison.

The next day, after 24 hours, we took out the recipient and checked that the bottom was still wet. The antenna could be removed without any problem and it was also quite wet inside (which means it was not completely dried), so it would be interesting to leave it longer. The good part is that the antenna has resisted and can be used for another test.

Figure 48: State of the cement after 24 h – Antenna removal.

4.5.3.1 Measurement results after 24 hours of drying

For this first time, the measurements were made manually, capturing the results of the network analyzer every hour. The gap between 9:15 p.m. (T9) and 9:15 a.m. (T21) is because it was left to dry during the night and measurements were taken again the next day until completing 24 hours. To avoid being present by taking measurements every hour, for the next test a MATLAB script has been prepared to take automatic measurements (see Annex C). In this way we can leave the antenna for a long time without needing to be physically there. After 24 hours of drying, the result is shown in Figure 49.

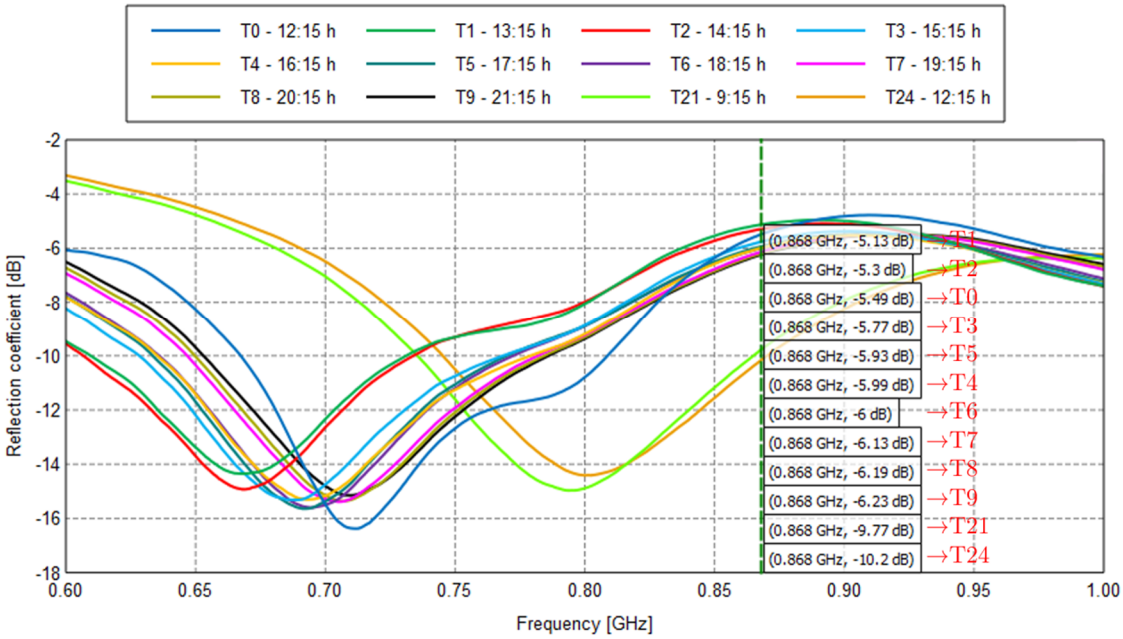

Figure 49: Reflection coefficient for 24 hours of drying – Measure based on w/c = 0.6 (reference impedance: 100 Ω).

Note that as the hours elapsed, the operating frequency shifted towards higher frequencies (except in the case of T0 → T1; possibly because the mixture had not yet settled the

ingredients until some time after), thus following the same trend discussed in Chapter 3. Furthermore, it is good to see that the reflection coefficient has a fairly stable value during the 24 hours of drying, with an average of about -15 dB of reflection coefficient that is a 96.8% of power delivered to the reader antenna (referenced to 100 Ω). However, working with a w/c = 0.6 for the experiment means more water than the used for the antenna design (w/c = 0.45) and then, leads to the set of measurements being slightly shifted to frequencies below 868 MHz.

4.5.3.2 Comparison with simulations based on w/c = 0.45

Next we are going to compare the measurements obtained with the simulation for w/c = 0.45. For reference, the parameters used in the simulation are collected in the Table 5.

		Fresh State	Setting State	Hardened State
Concrete (w/c = 0.45)	εr'	14	9	4
	tan δ	0.28	0.25	0.24
FR4	εr'	4		
	tan δ	0.03		

Table 5: Dielectric properties of the materials involved in the simulation for w/c = 0.45.

As we can see in Figure 50, a measure to represent each state during the drying process has been selected: measure T4 to fresh state, T9 to setting state and T24 to hardened state according to the hydration times in Figure 7.

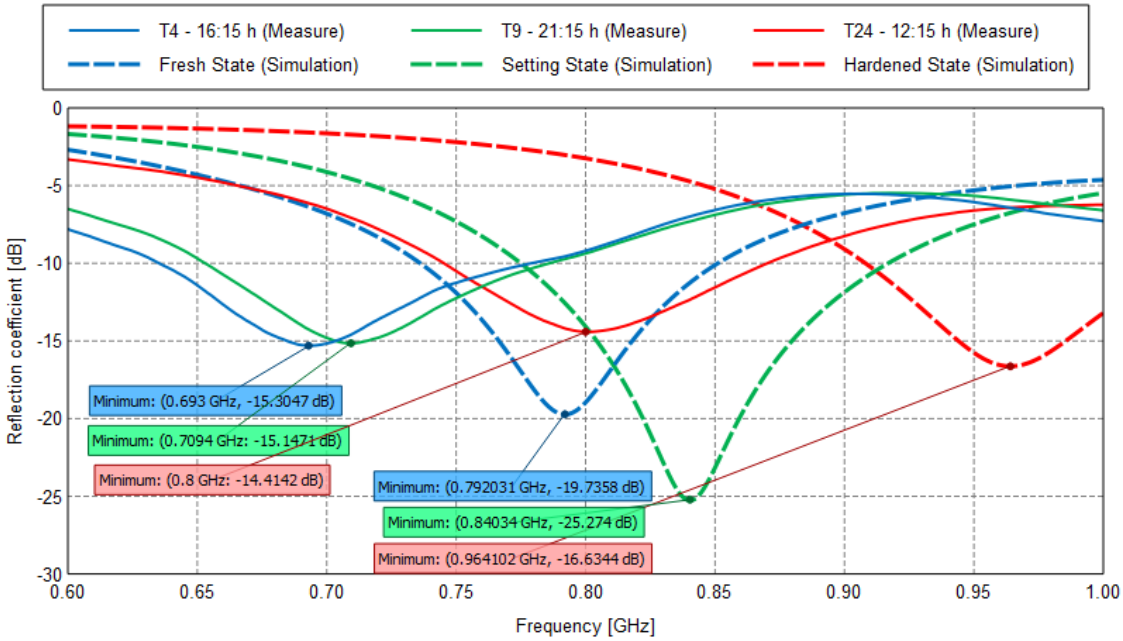

Figure 50: Reflection coefficient for the first 24 hours of drying – Simulation based on w/c = 0.45 against measures with w/c = 0.6 (reference impedance: 100 Ω).

For a better analyisis, Table 6 compares the frequency and reflection coefficient for each cement state (reference impedance: 100 Ω).

	Freq. shift after 24h[1]	**T4 vs Fresh S.**		**T9 vs Setting S.**		**T24 vs Hard. S.**	
		f [GHz]	**Γ [dB] (W_a[3])**	**f [GHz]**	**Γ [dB] (W_a)**	**f [GHz]**	**Γ [dB] (W_a)**
Simulation	≈ 172 MHz	0.792031	-19.7358 (98.9 %)	0.84034	-25.274 (99.7 %)	0.964102	-16.6344 (97.8 %)
Measure	≈ 107 MHz	0.693	-15.3047 (97.1 %)	0.7094	-15.1471 (96.9 %)	0.8	-14.4142 (96.4 %)
Deviation[2]	**65 MHz**	**0.099**	**(1.8 %)**	**0.130**	**(2.8 %)**	**0.164**	**(1.4 %)**

[1] For "Simulation" = frequency at Hardened State – frequency at Fresh State.
While for "Measure" = frequency at T24 – frequency at T4.
[2] Deviation = "Simulation" – "Measure".
[3] Power "accepted by" or delivered to the antenna.

Table 6: Simulation and measure comparison for a w/c = 0.45 and 0.6 respectively.

Although the reflection coefficient for simulation and measure seems quite different, as we see in Table 6, there is almost no difference in terms of power. The major difference is found for setting state, where T9 measure takes a reflection coefficient of -25.274 dB, this is a 99.7 % of power against -15.1471 dB for the simulated value that is a 96.9 %, i.e. a difference of 2.8 % which is practically the same. Concerning the operating frequency, there is a difference between both results about 100 – 150 MHz uniformly per state during the drying process, something that is easily variable with a change in the permittivity of the medium. The reason of this variation in frequency is mainly because the mixture made for the measures was waterier (w/c = 0.6) than for the simulation (w/c = 0.45) and that is why the set of simulated values, is at higher frequencies than the set of measures (against less water, the frequency increases). In order to determine the permittivity and conductivity (loss tangent) values for the concrete, we have to simulate a higher water content. Hence, for the next simulation, the electromagnetic properties of the concrete were modified according to Figure 7 for a w/c = 0.7 instead of w/c = 0.45.

4.5.3.3 Comparison with simulations based on w/c = 0.7

Based on Figure 7, the new parameters used in the simulation are gathered in the Table 7.

		Fresh State	**Setting State**	**Hardened State**
Concrete (w/c = 0.7)	εr'	26	20	12
	tan δ	0.30	0.37	0.35
FR4	εr'	4		
	tan δ	0.03		

Table 7: Dielectric properties of the materials involved in the simulation for w/c = 0.7.

Again, comparing T4, T9 and T24 with the simulation we obtain the results of Figure 51.

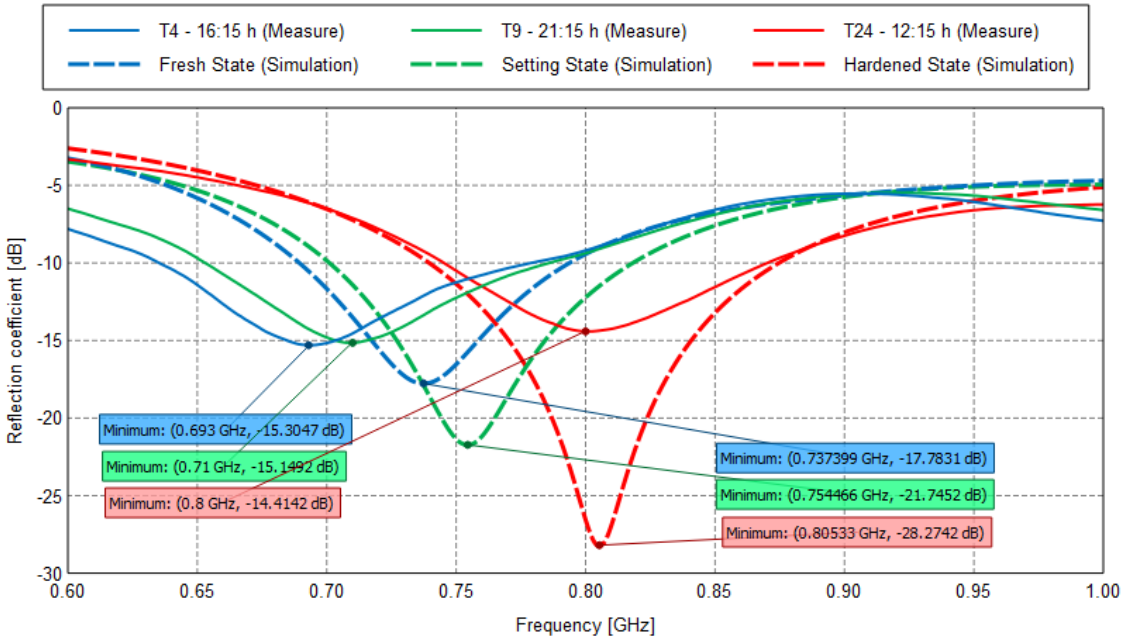

Figure 51: Reflection coefficient for the first 24 hours of drying – Simulation based on w/c = 0.7 against measures with w/c = 0.6 (reference impedance: 100 Ω).

We can see in advance that we have managed to reduce the deviation for the different cement states by increasing the simulated water content. Which confirms that the compound with which the experiment was carried out had a w/c closer to 0.7 than 0.45. If we compare Table 6 against Table 8 (both for reference impedance: 100 Ω), we see that we have succeeded in decreasing all deviations in terms of operating frequency and reflection coefficient but for the case of hardened state. In this case, the operating frequency is exactly the same as that of the measurement, but the reflection coefficient for the simulation has been reduced even further. Again, translated to power, we are talking about 99.9 % of delivered power against 96.4 %, that is a negligible difference.

	Freq. shift after 24h	**T4 vs Fresh S.**		**T9 vs Setting S.**		**T24 vs Hard. S.**	
		f [GHz]	**Γ [dB] (W_a)**	**f [GHz]**	**Γ [dB] (W_a)**	**f [GHz]**	**Γ [dB] (W_a)**
Simulation	≈ 68 MHz	0.737399	-17.7831 (98.3 %)	0.754466	-21.7452 (99.3 %)	0.80533	-28.2742 (99.9 %)
Measure	≈ 107 MHz	0.693	-15.3047 (97.1 %)	0.71	-15.1492 (96.9 %)	0.8	-14.4142 (96.4 %)
Deviation	**39 MHz**	**0.044**	**(1.2 %)**	**0.044**	**(2.4 %)**	**0.005**	**(3.5 %)**

Table 8: Simulation and measure comparison for a w/c = 0.7 and 0.6 respectively.

Nevertheless, since we are simulating a higher water content than for the measurements, we would expect to see the set of simulated values at lower frequencies than the measurements

and this is not the case. This leads to think that the room temperature or the container material may have played an important role when eliminating water (accumulating water on the surface and slowing down the drying process). Notice that in Figure 52 (a), the state of the cement after 24 h corresponded more to a setting state (compound still wet, darkly and easy to break) than to a hardened state like in the Figure 52 (b) (compound totally dry, light colour and difficult to destroy). Having more water content implies that the hydration time is longer than for the case of a w/c of 0.45 (there is more water to evaporate) and therefore, for a w/c of 0.6 would need more than 24 hours to reach a hardened state.

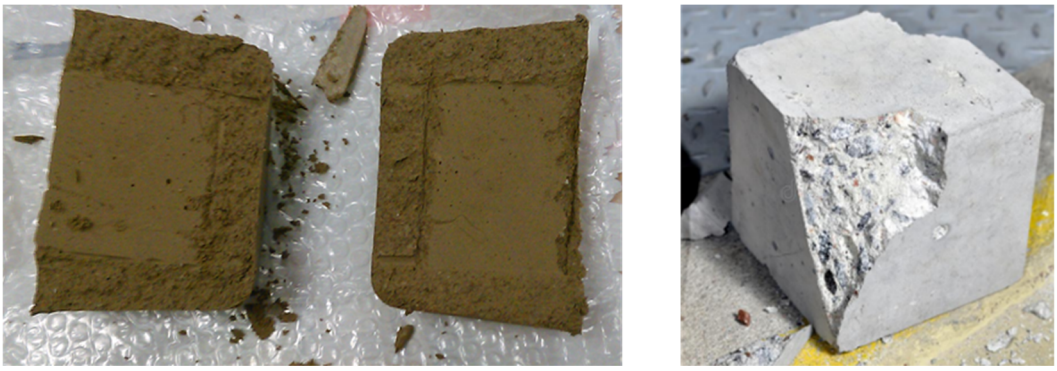

(a) Hardened state for the experiment (b) Dried cement sample

Figure 52: Hardened state comparison for cement blocks.

That is to say, for a w/c of 0.45 after 24 hours, the mixture should be waterless (or almost without water - see Figure 7 where the dielectric properties of the medium for w/c = 0.45 are stabilized in the last hours) and we probably would not be able to break the cement block with a regular hammer as we did for a w/c of 0.6. Even so, as 24 hours drying elapsed, we broke the cement block to check the status. It had not completely eliminated all the water and probably if we had continued monitoring the operating frequency, it would have continued to increase till it had no water.

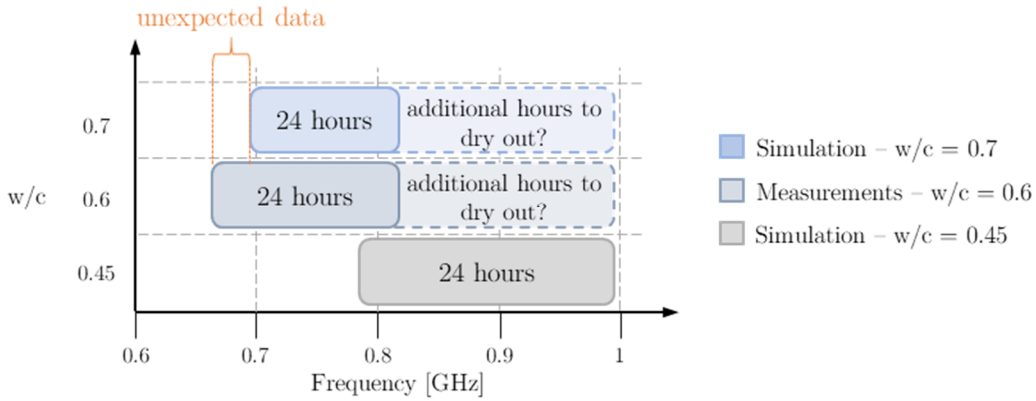

Figure 53: Simulations and measurements analysis in function of the w/c.

The explanation is roughly depicted in Figure 53, where “unexpected data” may be due to the effect of the container accumulating water on the surface, by deviation when calculating

the w/c of the experiment, by deviation of the parameters in the simulations, etc. And that it needs additional hours of drying makes sense because the operating frequency in the hardened state for w/c = 0.7 is about 800 MHz, but for w/c = 0.6 it has to be slightly higher and not be the same as it has less water content. It should also be taken into account that it is difficult to compare the temporal evolution between simulations and measurements because we do not know how the drying process was in the data we took as reference. And therefore, it can directly affect the drying process if we are not measuring under the same conditions.

4.5.3.4 Comparison with simulations at 868 MHz and $Z_0 = 50\ \Omega$

Given that the initial objective was to make an antenna to work well with a reference impedance of 50 Ω at 868 MHz, to finish, the results at 868 MHz for the antenna designed (w/c = 0.45) as well as the results for w/c = 0.6 and 0.7 are collected in Table 9. Then we can also see if the antenna designed at w/c = 0.45 still serves us to monitor a compound with w/c = 0.6 or 0.7. Those results are extracted from Figures 35 (c), 49 and 51.

		T4 vs Fresh S.	**T9 vs Setting S.**	**T24 vs Hard. S.**
		Γ [dB] (W_a)	Γ [dB] (W_a)	Γ [dB] (W_a)
[A]	**Simulation (w/c = 0.45)**	-6.95801 (79.9 %)	-13.438 (95.5 %)	-7.67115 (82.9 %)
[B]	**Measure (w/c = 0.6)**	-2.92 (48.9 %)	-3.09 (50.9 %)	-4.73 (66.3 %)
[C]	**Simulation (w/c = 0.7)**	-3.58 (56.1 %)	-3.95 (59.7 %)	-6.63 (78.3 %)
Deviation		**A-B = (31 %) C-B = (7.2 %)**	**A-B = (44.6 %) C-B = (8.8 %)**	**A-B = (16.6 %) C-B = (12 %)**

Table 9: Simulations and measure comparison at 868 MHz (reference impedance: 50 Ω).

As we can see in Table 9, the antenna designed to work with a w/c = 0.45 at 868 MHz works fairly uniformly for the 3 concrete states with 79.9% of transmitted power for the worst case. However, when using this antenna in a compound where the water content is higher than the expected (w/c = 0.6 or 0.7), the transmitted power is reduced, in particular for the fresh and setting states. Due to the fact that the state of the concrete when it is dry (hardened state) has the same electromagnetic properties regardless of the initial w/c, when the compound with w/c = 0.6 and 0.7 reaches the hardened state, the transmitted power increases. In consequence:

- The antenna designed to monitor a concrete with w/c = 0.45 can be used to monitor a period of time in the hardened state a concrete with w/c = 0.6 or 0.7 (in general, regardless of the initial w/c).
- To monitor the fresh and setting state of a concrete with higher water content (w/c = 0.6 or 0.7) than the one considered for the antenna design (w/c = 0.45), it will be necessary to design another antenna that covers that particular bandwidth. Because the higher the water content, the longer the drying time and therefore the longer the working frequency shifting (i.e., higher bandwidth).

4.6 Chapter Conclusions

At this point, we can conclude with some important observations for the next test:

1. After 24 h (T24), the compound was not able to evaporate all the water because the quantity of water content (and probably due to the plastic container – see point 2) and consequently, the state of the compound was more similar to the setting state than to the hardened state (see Figure 52). I.e., the higher the water content, the longer it will take for the compound to dry.
2. In addition, plastic containers instead of wood or directly the concrete on the floor for example, could slow down or speed up the drying process. When it is necessary, concrete experts use plastic to prevent water from filtering too quickly (water loss) [13].
3. By increasing the permittivity values for the simulation (higher amount of water) according to a w/c = 0.7, the measure and simulation results are more similar, which indicates that we used a mixture quite watery for the experiment or that in the experiment, the compound dried too slowly compared to the reference we took. In any case, it would be better to work with a lower w/c to speed up the drying process.
4. If after 24 h the cement is still fresh, it means that it has to be left longer to complete the drying process and see how far it moves in frequency. That is, leave it until a point where the frequency does not change as the hours advance.
5. The amount of water in the compound can easily alter the measurements and hence spoil the data transmission (see Table 9). This is, if excessive water is added, the antenna may not work in the desired band. For instance, if an antenna is designed to work at w/c = 0.45, it will not work well in the fresh state when w/c = 0.6 because the operating frequency is shifted towards lower frequencies for w/c = 0.6. An example can be found in Table 9; for a fresh state with a w/c = 0.45 the transmitted power is 79.9 % while with a w/c = 0.6 it is only 48.9 %. As the compound dries, the difference in the transmitted power of different w/c is smaller because it falls within the operating bandwidth (the common time period – hardened state) for different

w/c's. A solution could be to have different types of antennas depending on the w/c of the mix. Then, you can use the most convenient antenna for your specific structure. But as the hardened state is the same for all w/c, the particular design of the antenna would only be necessary if the first hours of drying wanted to be monitored (fresh and setting state). And therefore, it would be necessary to cover larger bandwidths.

6. Considering the previous point, as the antenna for this project was designed for a w/c = 0.45, it would be good to prepare the mixture thoroughly so that the water-cement ratio is 0.45. Hence, simulation and real result would cover the range of interest. In turn, we could detect if there are variances (between reference data and measurements) by drying conditions like temperature, container used, humidity, etc.
7. For the next experiment, measurements should be performed on concrete instead of cement in order to discard possible deviations introduced by sand or gravel.
8. It is worth to automate measures to avoid having to be present.

Chapter 5

Conclusions and Future Work

5.1 Conclusions

This thesis has analysed the problem of working with an antenna in the UHF band at 868 MHz embedded in concrete, where the permittivity and the loss tangent vary over time. For this purpose, a value of permittivity and loss tangent at 868 MHz has been determined, evaluating information as a function of time and water content. Given that the electromagnetic properties are variable over time, it has been necessary to classify the drying process of the concrete by different states: fresh state, setting state and hardened state. With this, it has been possible to associate characteristics of the medium for the different states and thus cover with the simulations from the beginning to the end of the drying process. Thanks to this first analysis, two important aspects have been seen: the impact that the quantity of water in a concrete mixture has on the properties of the medium, and the progress of these during the drying process by eliminating water from the mixture. From this, we conclude that the greater the quantity of water, the greater the permittivity and loss tangent, and therefore, the greater the signal blockage when passing through the concrete.

Once the properties of the medium have been analysed and with the aim of understanding how the link losses change due to variations in complex permittivity, different scenarios have been proposed for different parameters in question such as antenna depth, length or cover thickness. Before we can evaluate these scenarios, a figure of merit is required to help us judge how good the link is and therefore the antenna pair gain has been presented, a factor that models the set of gains and propagation losses. Using this figure of merit, we have understood the behaviour of the concrete when an antenna is placed inside it.

The depth to which the antenna will fall into the concrete is something that cannot be controlled, however, we have seen that we are interested in having it in somehow as close as possible to the surface for a better link performance. Regarding the length of the antenna, we have seen the compromise that has to choose an appropriate size to cover in a stable way the three states of the concrete, being convenient to define a length of 6 cm. This is a value that slightly exceeds the specifications, but given the application, 1 cm is a difference that has been considered irrelevant. Adding a cover is mandatory, because the antenna will be in

contact with water and needs something to protect it, so we have analysed different cover thicknesses, seeing how this impacts on the link. From this we conclude that there is an improvement in widening the cover, but there comes a point where it is not worth making it thicker as we would be spoiling the antenna in terms of size for too little benefit.

Finally, because of the need to have a more real scenario, we moved from a multi-layer model to a finite model where the difference is demonstrated to be practically insignificant. This is good because with a multilayer model the computational cost of simulation is very low compared to a finite model and as we have seen, it is still a good reference. These last points have given the necessary knowledge to design the antenna in a way that reduces the dependence on complex permittivity, that is, with an antenna pair gain as uniform as possible during the drying process.

When designing the antenna, it has been necessary to use transmission lines to connect the dipole to the network analyzer upon its submersion, which has lead to the necessity of impedance matching to minimize the signal reflection. The quarter-wave transformer has been the best solution because of its simple and useful impedance matching circuit. With the design made, it has been adjusted until achieving more realistic conditions and without losing the matching, achieving a model capable of covering the 868 MHz band for any state of the concrete and feasible to replicate in the reality.

Later on, the antenna designed in FEKO has been fabricated to compare measurements and simulations to see how far we are from the reality of our study. Having the possibility to make measurements in the laboratory has been useful to learn the practical side of this work, and to see the previous preparation that it entails. In order to exclude possible deviations introduced by the antenna, we have compared the antenna in free space where the result has been quite satisfactory. With these measurements, the antenna has been sealed and immersed in concrete where the last measurements have been collected. For the experiment, a compound with a w/c = 0.6 was elaborated and therefore something waterier than the value we used for the simulation (w/c = 0.45), nevertheless, it already served us to assess the trend.

For the collection of results, the measurements were taken manually, but with the experience of this first test, a MATLAB script has been prepared to automate the collection of measurements every hour. Since our study was focused on the analysis of the first 24 hours of drying, after 24 hours we broke the cement block. Apparently, the state turned out to be more like a setting state than a hardened state because the water content required more than 24 hours to dry the compound completely. Apart from the excess water, it is possible that the drying process was slower than expected because of the container used in the experiment or because there were other environmental conditions to obtain the reference data. To verify this, a higher water content was simulated, where it was seen that the simulation and measurements were quite similar, following the same trend as the hours went by. This

justifies that the water content for the experiment was closer to 0.7 than 0.45. Also, with this comparison, it was possible to approximate certain parameters of interest such as the value of the permittivity and loss tangent for each state of the concrete.

As the amount of water in the compound can easily alter the measurements and hence spoil the data transmission, depending on the w/c we should use a different antenna devoted for that particular quantity of water, otherwise, the antenna might not work well in the fresh or setting state. It has been demonstrated that the antenna designed at w/c = 0.45 transmits with a power of 79.9 % for fresh state, 95.5 % for setting state and 82.9 % for hardened state. And that if this antenna is immersed in a w/c = 0.6, the power transmitted for the fresh state and setting state is 48.9 % and 50.9 % respectively, however, it is somewhat better for the hardened state that reach 66.3 %. Basically because, the state of the concrete when it is dried out is the same for all compounds regardless of their w/c, and that is why the necessity of a particular antenna design (depending the w/c) would only be applicable in case we wanted to monitor the fresh or setting state. In other words, the higher the w/c, the longer the drying process and hence, the greater the bandwidth that needs to be covered to monitor the concrete. Additionally, it has been learned that temporal comparison of measurements and simulations can lead to deviations if the conditions of the drying process for the reference data are unknown. Mainly because factors such as temperature, or the place where the concrete is drying can be crucial, speeding up or slowing down the drying process.

5.2 Future Work

With the design of an antenna prepared to monitor the status of a regular concrete of w/c = 0.45 ends this thesis. Despite the main topics have been addressed, other more general research lines can be devised, and they are listed below.

- Leave different compounds with different w/c dry until they have no water at all to see if the operating frequency for hardened state is the same for all of them. In this way it is verified that if the user uses an antenna prepared to work with w/c = 0.7 for example, it could also serve to measure a concrete with w/c = 0.6 or 0.45 since the bandwidth for w/c = 0.7 includes the bandwidth for w/c = 0.6 and 0.45.

- Connect an EM4325 chip to obtain parameters of interest such as humidity, temperature, etc. In turn, see how the presence of the chip on the antenna affects.

- Designing the antenna inside a spherical hull in order to improve its design for the application. In this way the antenna is best suited to be immersed in the concrete.

- Test in a real case. Place the antenna with the sensor inside the concrete and with a reader outside capture the data.

- Investigate and extend the use case for other compounds and applications.

References

[1] J. Zhang, B. Huang, G. Zhang, and G. Y. Tian, "Wireless passive ultra high frequency RFID antenna sensor for surface crack monitoring and quantitative analysis," *Sensors (Switzerland)*, vol. 18, no. 7, pp. 2130-1-2130–11, 2018, doi: 10.3390/s18072130.

[2] J. Gemio, J. Parron, and J. Soler, "Human body effects on implantable antennas for ISM bands applications: Models comparisaon and propagation losses study," *Prog. Electromagn. Res.*, vol. 110, pp. 437–452, 2010, doi: 10.2528/PIER10102604.

[3] B. Abdelwahed, "A review on building progressive collapse, survey and discussion," *Case Stud. Constr. Mater.*, vol. 11, 2019, doi: 10.1016/j.cscm.2019.e00264.

[4] M. Hamma-adama and T. Kouider, "Causes of building failure and collapse in Nigeria: Professionals' view," *Am. J. Eng. Res.*, no. 6, pp. 289–300, 2017.

[5] A. G. Batrakova and O. Gredasova, "Influence of road conditions on traffic safety," *Procedia Eng.*, vol. 134, pp. 196–204, 2016, doi: 10.1016/j.proeng.2016.01.060.

[6] G. Marrocco, "Pervasive electromagnetics: Sensing paradigms by passive RFID technology," *IEEE Wirel. Commun.*, vol. 17, no. 6, pp. 10–17, 2010, doi: 10.1109/MWC.2010.5675773.

[7] S. Manzari and G. Marrocco, "Modeling and applications of a chemical-loaded UHF RFID sensing antenna with tuning capability," *IEEE Trans. Antennas Propag.*, vol. 62, no. 1, pp. 94–101, 2014, doi: 10.1109/TAP.2013.2287008.

[8] Z. Meng and Z. Li, "RFID tag as a sensor - A review on the innovative designs and applications," *Meas. Sci. Rev.*, vol. 16, no. 6, pp. 305–315, 2016, doi: 10.1515/msr-2016-0039.

[9] E. Microelectronic, "Technical specification sheet for 18000-63 Type C (Gen2) and 18000-63 Type C / 18000-64 Type D (Gen2 / TOTAL) RFID IC EM4325," pp. 1–67, 2015.

[10] N. P. Bhatta and M. Geethapriya, "RADAR and its applications," *Int. Sci. Press*, vol. 10, no. 3, pp. 1–9, 2017.

[11] P. Swallow, "Practical VHF/UHF Antennas," *Radio Commun. Handb.*, pp. 1–38, 2011.

[12] A. Cardama Aznar, L. Jofre Roca, J. M. Rius Casals, J. Romeu Robert, S. Blanch Boris, and M. Ferrando Bataller, *Antenas*, 2nd Ed. Barcelona, Spain: Edicions UPC, 2002.

[13] T. Hirschi, H. Knauber, M. Lanz, J. Schrabback, C. Spirig, and U. Waeber, "Concrete Handbook," *Constr. Sika*, pp. 1–147, 2005.

[14] N. Makul, "Dielectric permittivity of various cement-based materials during the first

24 hours hydration," *Open J. Inorg. Non-metallic Mater.*, vol. 3, no. 4, pp. 53–57, 2013, doi: 10.4236/ojinm.2013.34009.

[15] J. Martinez-Vega, *Dielectric Materials for Electrical Engineering*, 1st Ed. London, United Kingdom: ISTE Ltd and John Wiley & Sons Inc, 2010.

[16] K. C. G. Ong and A. Akbarnezhad, *Microwave-Assisted Concrete Technology*, 1st Ed. Boca Ratón, United States: CRC Press, 2015.

[17] C. A. Balanis, *Advanced Engineering Electromagnetics*, 2nd Ed. New York, United States: John Wiley & Sons, Inc., 2012.

[18] D. M. Pozar, *Microwave Engineering*, 4th Ed. New York, United States: John Wiley & Sons, Inc, 2011.

[19] EMSS, "FEKO User's Manual," *EM Softw. Syst. Ltd*, 2014, [Online]. Available: www.feko.info.

[20] RF Café contributors, "Dielectric Constant, Stength, & Loss Tangent", *RF Café*, 2020. <https://www.rfcafe.com/references/electrical/dielectric-constants-strengths.htm#:~:text=The dielectric loss tangent is,the lossiness of the medium.> (accessed Jun. 06, 2020).

[21] C. C. Solutions, "SMA 50 ohm end launch jack receptacle - round contact," *Components*, vol. 48, pp. 48–51, 2020.

[22] A. Technologies, "Agilent PNA-X Series Microwave Network Analyzers," *Serv. Guid.*, pp. 1–36, 2014.

[23] Rohde & Schwarz, "Measuring Balanced Components with Vector Network Analyzer ZVB," *1Ez53*, pp. 1–19, 2004.

[24] G. Beziuk, P. P. Jarzab, K. Nowak, E. F. Plinski, M. J. Walczakowski, and J. S. Witkowski, "Dielectric properties of the FR-4 substrates in the THz frequency range," *Int. Conf. Infrared, Millimeter, Terahertz Waves, IRMMW-THz*, no. 2, pp. 4–5, 2012, doi: 10.1109/IRMMW-THz.2012.6380160.

[25] OK Diario contributors, "Cómo hacer cemento paso a paso", *OK Diario*, 4 April 2018. <https://okdiario.com/howto/como-hacer-cemento-paso-paso 2058099#:~:text=Para%20hacer%20el%20cemento%2C%20coge,evitar%20la%20formaci%C3%B3n%20de%20grumos.> (accessed Jun. 06, 2020)

Annex

A Propagation Analysis: Test Plan

Antenna Pair Gain	S-Parameters			Distance Embedded Dipole	Dielectric Constant	Concrete Loss tangent	
(Ga [dB])	S21 [dB]	S11 [dB]	S22 [dB]	H2 [cm]	εr'	tan δ	
-35,00265524	-35,2539	-15,1451	-15,7783	2	14	0,28	Fresh State
-36,7507374	-36,9985	-15,1252	-15,9325	4			
-38,6256714	-38,8481	-15,1346	-17,0162	6			
-40,19638744	-40,437	-15,1321	-16,2059	8			
-41,9860459	-42,2154	-15,1311	-16,6928	10			
-43,64411016	-43,8792	-15,1335	-16,4352	12			
-45,36630803	-45,5989	-15,131	-16,5475	14			
-47,05990743	-47,2932	-15,133	-16,5139	16			
-48,75858549	-48,992	-15,1316	-16,5105	18			
-50,45849154	-50,6915	-15,1324	-16,5272	20			
-32,36129293	-32,5092	-15,165	-25,0376	2	9	0,25	Setting State
-33,41770737	-33,6098	-15,149	-18,8235	4			
-35,08932559	-35,2668	-15,1321	-20,1492	6			
-36,35807253	-36,5247	-15,1557	-21,3336	8			
-37,60647787	-37,7835	-15,1445	-20,1554	10			
-39,00753093	-39,1812	-15,1413	-20,5254	12			
-40,30536325	-40,477	-15,1501	-20,7263	14			
-41,61043234	-41,785	-15,1443	-20,4157	16			
-42,95002379	-43,1232	-15,1446	-20,5691	18			
-44,254498	-44,4274	-15,1475	-20,5898	20			
-28,08577822	-28,4258	-15,169	-13,3443	2	4	0,24	Hardened State
-28,81495357	-29,1529	-15,2247	-13,3513	4			
-29,79549802	-30,1843	-15,1477	-12,4561	6			
-30,94431057	-31,3628	-15,105	-12,0108	8			
-31,977123	-32,3803	-15,1437	-12,2261	10			
-32,8725606	-33,2562	-15,1786	-12,5263	12			
-33,78145042	-34,1684	-15,16	-12,4805	14			
-34,76288572	-35,1612	-15,1343	-12,3079	16			
-35,74584777	-36,1443	-15,1418	-12,3019	18			
-36,68269044	-37,0747	-15,1595	-12,3971	20			

Table 10: Ga vs H2 in function of εr' and tan δ – See Figure 12

Antenna Pair Gain	S-Parameters			Length Embedded Dipole	Dielectric Constant	Concrete Loss tangent	Distance Embedded Dipole	
(Ga [dB])	S21 [dB]	S11 [dB]	S22 [dB]	L2 [cm]	εr'	tan δ	H2 [cm]	
-45,47679809	-48,2769	-15,1363	-3,3855	2	14	0,28	6	Fresh State
-41,78507911	-43,0117	-15,1363	-6,5321	3				
-39,66775162	-40,0386	-15,1376	-12,7713	4				
-38,51636278	-38,7437	-15,1399	-16,7730	5				
-37,96720298	-38,4051	-15,1422	-11,7153	6				
-37,77961281	-38,4610	-15,1442	-9,2726	7				
-37,83407294	-38,6676	-15,1460	-8,2798	8				
-38,11926097	-38,9838	-15,1477	-8,1060	9				
-38,70364681	-39,4740	-15,1495	-8,6600	10				
-44,01832612	-48,6202	-15,145	-1,9214	2	9	0,25	6	Setting State
-40,04866377	-42,6674	-15,143	-3,6096	3				
-37,50278713	-38,5484	-15,139	-7,2323	4				
-35,87184064	-36,0972	-15,134	-16,875	5				
-34,90020483	-35,1362	-15,132	-16,399	6				
-34,36606563	-35,0108	-15,132	-9,5593	7				
-34,11284562	-35,1909	-15,133	-7,0967	8				
-34,04591855	-35,4401	-15,1331	-5,9922	9				
-34,11666496	-35,6824	-15,1334	-5,5187	10				
-43,73541551	-51,9569	-15,152	-0,7332	2	4	0,24	6	Hardened State
-39,51804759	-45,9356	-15,154	-1,1654	3				
-36,51032149	-41,276	-15,158	-1,8327	4				
-34,22734879	-37,3374	-15,163	-3,0452	5				
-32,4900681	-34,0673	-15,169	-5,4865	6				
-31,18888135	-31,6987	-15,168	-10,817	7				
-30,2411397	-30,4544	-15,157	-17,455	8				
-29,58341333	-30,1529	-15,1422	-10,2134	9				
-29,14247399	-30,3475	-15,1287	-6,6094	10				

Table 11: Ga vs L2 in function of εr' and tan δ – See Figure 14

Antenna Pair Gain	S-Parameters			Dielectric Constant	Loss tangent	Drying hours	Concrete State	Distance Embedded Dipole	Embedded Dipole Length
(Ga [dB])	S21 [dB]	S11 [dB]	S22 [dB]	εr'	tan δ	h	-	H2 [cm]	L2 [cm]
-39,60176654	-40,023	-15,159	-11,942	15	0,33	0	Fresh State	6	6
-37,96720298	-38,405	-15,142	-11,715	14	0,28	3			
-36,37033789	-36,815	-15,123	-11,637	13	0,23	6	Setting State		
-34,48457099	-34,621	-15,154	-34	7	0,28	9			
-31,33410462	-31,662	-15,086	-13,671	6	0,16	12	Hardened State		
-32,70404287	-34,231	-15,174	-5,6171	4	0,25	15			
-34,18147808	-36,775	-15,22	-3,6393	3	0,33	18			
-31,8621629	-32,604	-15,13	-8,8516	5	0,2	21			
-31,8621629	-32,604	-15,13	-8,8516	5	0,2	24			
-19,55603533	-42,809	-14,852	-0,0213	-	-	-	Scenario in Free Space	6	6

Table 12: Ga vs εr' or h with H2, L2 fixed – See Figure 15

Antenna Pair Gain	S-Parameters			Dielectric Constant	Loss tangent	Drying hours	Concrete State	Distance Embedded Dipole	Embedded Dipole Length	
(Ga [dB])	S21 [dB]	S11 [dB]	S22 [dB]	εr'	tan δ	h	-	H2 [cm]	L2 [cm]	
-38,51527313	-38,724	-15,157	-17,694	15	0,33	0	Fresh State	6	6	Multilayer model with coating of 1mm on embedded
-37,12761825	-37,36	-15,139	-16,568	14	0,28	3				
-35,74873737	-36,013	-15,117	-15,357	13	0,23	6	Setting State			
-33,82296625	-34,573	-15,158	-9	7	0,28	9				
-30,87005607	-32,345	-15,097	-5,7648	6	0,16	12	Hardened State			
-31,80487635	-34,363	-15,177	-3,6879	4	0,25	15				
-33,01817533	-36,242	-15,221	-2,9313	3	0,33	18				
-31,20017325	-33,153	-15,136	-4,6607	5	0,2	21				
-31,20017325	-33,153	-15,136	-4,6607	5	0,2	24				
-38,36280449	-39,266	-15,155	-7,9005	15	0,33	0	Fresh State	6	6	Multilayer model with coating of 2mm on embedded dipole
-36,98567313	-37,942	-15,136	-7,6368	14	0,28	3				
-35,62178414	-36,644	-15,115	-7,3357	13	0,23	6	Setting State			
-33,45802795	-35,162	-15,162	-5	7	0,28	9				
-30,574791	-33,105	-15,102	-3,7295	6	0,16	12	Hardened State			
-31,19432526	-34,563	-15,177	-2,7971	4	0,25	15				
-32,18809825	-35,972	-15,221	-2,4519	3	0,33	18				
-30,76433778	-33,692	-15,139	-3,2398	5	0,2	21				
-30,76433778	-33,692	-15,139	-3,2398	5	0,2	24				
-38,13503852	-40,782	-15,153	-3,5729	15	0,33	0	Fresh State	6	6	Multilayer model with coating of 4mm on embedded dipole
-36,7738917	-39,456	-15,134	-3,5289	14	0,28	3				
-35,43243487	-38,161	-15,113	-3,4726	13	0,23	6	Setting State			
-32,92301486	-36,27	-15,166	-3	7	0,28	9				
-30,14856402	-34,229	-15,106	-2,2422	6	0,16	12	Hardened State			
-30,2768689	-34,913	-15,177	-1,9019	4	0,25	15				
-30,88762961	-35,69	-15,222	-1,8123	3	0,33	18				
-30,12554394	-34,496	-15,141	-2,0561	5	0,2	21				
-30,12554394	-34,496	-15,141	-2,0561	5	0,2	21				
⋮						⋮				⋮
-37,8192325	-42,863	-15,152	-1,6935	15	0,33	0	Fresh State	6	6	Multilayer model with coating of 8mm on embedded dipole
-36,48213628	-41,504	-15,134	-1,7042	14	0,28	3				
-35,17318133	-40,177	-15,113	-1,7135	13	0,23	6	Setting State			
-32,16439958	-37,732	-15,169	-1	7	0,28	9				
-29,567002	-35,574	-15,108	-1,3006	6	0,16	12	Hardened State			
-28,88683368	-35,416	-15,177	-1,1314	4	0,25	15				
-28,716127	-35,458	-15,222	-1,0697	3	0,33	18				
-29,21635865	-35,495	-15,141	-1,2093	5	0,2	21				
-29,21635865	-35,495	-15,141	-1,2093	5	0,2	24				
-37,69935466	-43,555	-15,152	-1,354	15	0,33	0	Fresh State	6	6	Multilayer model with coating of 10mm on embedded dipole
-36,37170888	-42,185	-15,134	-1,37	14	0,28	3				
-35,07552966	-40,845	-15,113	-1,3865	13	0,23	6	Setting State			
-31,86115604	-38,234	-15,169	-1	7	0,28	9				
-29,34218737	-36,024	-15,109	-1,0877	6	0,16	12	Hardened State			
-28,28097642	-35,605	-15,177	-0,9204	4	0,25	15				
-27,63919432	-35,402	-15,221	-0,8227	3	0,33	18				
-28,84811556	-35,84	-15,141	-1,003	5	0,2	21				
-28,84811556	-35,84	-15,141	-1,003	5	0,2	24				

Table 13: Ga vs εr' or h with H2, L2 fixed in function of coating thickness – See Figure 15

Antenna Pair Gain	S-Parameters			Dielectric Constant	Loss tangent	Drying hours	Concrete State	Distance Embedded Dipole	Embedded Dipole Length	
(Ga [dB])	S21 [dB]	S11 [dB]	S22 [dB]	εr'	tan δ	h	-	H2 [cm]	L2 [cm]	
-38,36280449	-39,266	-15,155	-7,9005	15	0,33	0	Fresh State	6	6	Coating of 2mm on infinite block of concrete
-36,98567313	-37,942	-15,136	-7,6368	14	0,28	3				
-35,62178414	-36,644	-15,115	-7,3357	13	0,23	6	Setting State			
-33,45802795	-35,162	-15,162	-5	7	0,28	9				
-30,574791	-33,105	-15,102	-3,7295	6	0,16	12	Hardened State			
-31,19432526	-34,563	-15,177	-2,7971	4	0,25	15				
-32,18809825	-35,972	-15,221	-2,4519	3	0,33	18				
-30,76433778	-33,692	-15,139	-3,2398	5	0,2	21				
-30,76433778	-33,692	-15,139	-3,2398	5	0,2	24				
-38,3260642	-39,227	-15,157	-7,9097	15	0,33	0	Fresh State	6	6	Coating of 2mm on 20cm block of concrete
-36,76949498	-37,722	-15,12	-7,6595	14	0,28	3				
-35,15025358	-36,167	-15,068	-7,37	13	0,23	6	Setting State			
-33,21554099	-34,907	-15,121	-5	7	0,28	9				
-29,39046907	-31,887	-15,263	-3,7677	6	0,16	12	Hardened State			
-31,60743923	-34,999	-15,092	-2,7788	4	0,25	15				
-32,5732503	-36,363	-15,18	-2,4483	3	0,33	18				
-30,39645253	-33,337	-15,246	-3,2218	5	0,2	21				
-30,39645253	-33,337	-15,246	-3,2218	5	0,2	24				
⋮						⋮				⋮
-37,69935466	-43,555	-15,152	-1,354	15	0,33	0	Fresh State	6	6	Coating of 10mm on infinite block of concrete
-36,37170888	-42,185	-15,134	-1,37	14	0,28	3				
-35,07552966	-40,845	-15,113	-1,3865	13	0,23	6	Setting State			
-31,86115604	-38,234	-15,169	-1	7	0,28	9				
-29,34218737	-36,024	-15,109	-1,0877	6	0,16	12	Hardened State			
-28,28097642	-35,605	-15,177	-0,9204	4	0,25	15				
-27,63919432	-35,402	-15,221	-0,8227	3	0,33	18				
-28,84811556	-35,84	-15,141	-1,003	5	0,2	21				
-28,84811556	-35,84	-15,141	-1,003	5	0,2	24				
-37,6636893	-43,513	-15,155	-1,3563	15	0,33	0	Fresh State	6	6	Coating of 10mm on 20cm block of concrete
-36,15695755	-41,96	-15,118	-1,374	14	0,28	3				
-34,60451138	-40,364	-15,067	-1,3907	13	0,23	6	Setting State			
-31,63074012	-37,969	-15,129	-1	7	0,28	9				
-28,15701902	-34,81	-15,273	-1,0943	6	0,16	12	Hardened State			
-28,67305995	-36	-15,091	-0,9096	4	0,25	15				
-28,02969829	-35,794	-15,18	-0,8226	3	0,33	18				
-28,45572797	-35,495	-15,247	-0,9898	5	0,2	21				
-28,45572797	-35,495	-15,247	-0,9898	5	0,2	24				

Table 14: Ga vs εr' or h with H2, L2 fixed in function of concrete block – See Figure 20

B Fabricated Antenna: Size Details

In order to have a comparison against the infinity model (Figure 29 (a)), the dimensions of the fabricated antenna are given below. Basically with regards to the previous designed model, the length of the $\lambda/4$ lines has been reduced (from 4.2 to 3.6 cm). As discussed in equation 24, the length for a $\lambda/4$ transmission line in a medium is dependent on the permittivity of the medium. Using a permittivity value not very close to 14 (fresh state) or very close to 4 (hardened state), the antenna works more or less well for all concrete states. In equation 24, a value of 6.05 was recommended due to the effect of FR4 together with the concrete, and in this case a value of 5.8 is used giving a length of 3.6 cm for the $\lambda/4$ transmission lines. Also, narrowing the last section that connects to the feeding point has also made the transition of currents smoother, giving a better final result. Notice that with this adjustment, the antenna exhibits a good matching for the three concrete states covering the band of interest.

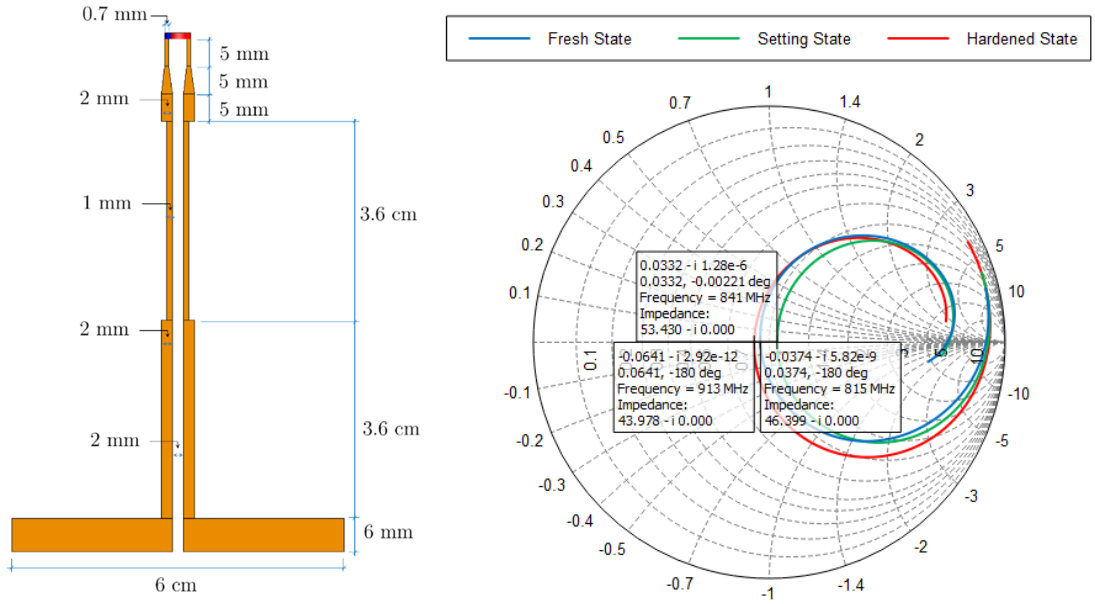

(a) Dipole and Transmission Line Sizes (b) Impedance

Figure 54: Dipole and its transmission line details after the adjustment for finite model.

C Automated Measurements

To avoiding the collection of results manually, a script was prepared that allows:

1. Connect to the network analyzer remotely.
2. Define how often the results are collected.
3. Store ".s1p" files compatibles with FEKO.

The code is given below.

```
% ########## Automated Measurements for Concrete Status Monitoring ##########
%
%*************************************************************************
%                                                                        *
% Filename:       PNA_X_TCPIP_AutomatedMeasurements.m                    *
% Description:    The purpose of this file is to automate the collection of *
%                 measurements from the PNA-X. To do this, communication is *
%                 established with the instrument, the data read from the   *
%                 instrument is written to a file and the connection with   *
%                 the instrument is closed. After 1 hour, the process is    *
%                 repeated until completing 48 hours (2 days).              *
%                                                                        *
% Author:         Javier Colin Pérez                                     *
% Created:        03-Mar-2020                                            *
%                                                                        *
%*************************************************************************

clear all      % Removes all variables from the current workspace,
close all      % Deletes all figures whose handles are not hidden

% Create a VISA (Virtual Instrument Standard Architecture)
% connection to interface with instrument
vt = visa('agilent', 'TCPIP::158.109.73.191::INSTR');      % Create a VISA-TCPIP object
                                                           % connected to an instrument
                                                           % configured with IP address
                                                           % 158.109.73.191

%vu = visa('agilent', 'USB0::0x0957::0x0118::MY49421580::0');      % Create a VISA-USB
                                                                   % object connected to %
                                                                   a USB instrument
                                                                   % with manufacturer ID
                                                                   % 0x0957, model code
                                                                   % 0x0118, and serial
                                                                   % number MY49421580

% Set up connection parameter for transfer of measurement
% data from the instrument
np = 1001;     % np = number of points

vt.InputBufferSize = 20*np*3;        % Specifies the total number of bytes that can be
                                     % stored in the software input buffer during a read
                                     % operation: 20*1001 -> (# freq. points)*(freq +
                                     % abs + ang) characters

% Create a loop to monitor the concrete state each hour
N = 2*12;      % 'N' is the number of hours we want to monitor the concrete: 2*12 ->
               % (days)*(hours per day) hours

for i = 0:1:N-1       % For each hour, read data and save it into a .txt file

    % Connect interface object to instrument
    fopen(vt);        % Connects 'vt' to the instrument

    % Write data to the instrument
    fprintf(vt,'CALC:PAR:MNUM 1');   % Select trace 1 channel 1
    fprintf(vt,'CALC:DATA:SNP:PORTs? "1"');         % Request 1-port measurement data
                                                    % from instrument
```

```
    % Read data from instrument
    bla = fscanf(vt);         % Reads data from the instrument connected to 'vt' object,
                              % and returns it to 'bla' variable

    % Disconnect interface object from instrument
    fclose(vt);       % Disconnects 'vt' object from the instrument

    % Prepare data for graphing/store
    x = str2num(bla);         % Convert 'bla' string to numeric array
    y = reshape(x, 1001, 3);         % Reshape array 'x'
    f = y(:,1);       % Access to all elements on the first column of 'y' matrix
    mag_dB = y(:,2);  % Access to all elements on the second column of 'y' matrix
    ph_deg = y(:,3);  % Access to all elements on the third column of 'y' matrix



    % Display data from instrument
    %subplot(2, 1, 1);plot(f, mag_dB);       % Figure with two stacked subplots (subplot %
                                             1). Plot 'mag_dB' in function of 'f'

    %subplot(2, 1, 2);plot(f, ph_deg);       % Figure with two stacked subplots (subplot
                                             % 2). Plot 'ph_deg' in function of 'f'

    % Store/Write the data in a .s1p file
    filename = sprintf('Data_T%d.s1p', i);   % Format data into string or character
                                             % vector

    fid = fopen(filename,'w');       % Open or create new file for writing. Discard
                                     % existing contents, if any

    fprintf(fid,'# Hz S  dB   R 100\n');     % Write data to text file. Header reference
                                             % 100 ohm (differential)

    for cont=1:np,
        fprintf(fid,'%.2f %f %f\n',f(cont),mag_dB(cont),ph_deg(cont));    % Write the
                                                                          % data (f,
                                                                          % mag_dB,
                                                                          % ph_deg) for
                                                                          % each and
                                                                          % every point
                                                                          % in the file
    end;
    fclose(fid);      % Closes an open file

    pause(3600);      % Pauses execution for 3600 seconds (1 hour) before continuing and
                      % then, connect again to to the instrument to obtain new data
end
```